A measurement of R_b using a double tagging method

The OPAL Collaboration

G. Abbiendi[2], K. Ackerstaff[8], G. Alexander[23], J. Allison[16], N. Altekamp[5], K.J. Anderson[9], S. Anderson[12], S. Arcelli[17], S. Asai[24], S.F. Ashby[1], D. Axen[29], G. Azuelos[18,a], A.H. Ball[17], E. Barberio[8], R.J. Barlow[16], R. Bartoldus[3], J.R. Batley[5], S. Baumann[3], J. Bechtluft[14], T. Behnke[27], K.W. Bell[20], G. Bella[23], A. Bellerive[9], S. Bentvelsen[8], S. Bethke[14], S. Betts[15], O. Biebel[14], A. Biguzzi[5], S.D. Bird[16], V. Blobel[27], I.J. Bloodworth[1], M. Bobinski[10], P. Bock[11], J. Böhme[14], D. Bonacorsi[2], M. Boutemeur[34], S. Braibant[8], P. Bright-Thomas[1], L. Brigliadori[2], R.M. Brown[20], H.J. Burckhart[8], C. Burgard[8], R. Bürgin[10], P. Capiluppi[2], R.K. Carnegie[6], A.A. Carter[13], J.R. Carter[5], C.Y. Chang[17], D.G. Charlton[1,b], D. Chrisman[4], C. Ciocca[2], P.E.L. Clarke[15], E. Clay[15], I. Cohen[23], J.E. Conboy[15], O.C. Cooke[8], C. Couyoumtzelis[13], R.L. Coxe[9], M. Cuffiani[2], S. Dado[22], G.M. Dallavalle[2], R. Davis[30], S. De Jong[12], L.A. del Pozo[4], A. de Roeck[8], K. Desch[8], B. Dienes[33,d], M.S. Dixit[7], J. Dubbert[34], E. Duchovni[26], G. Duckeck[34], I.P. Duerdoth[16], D. Eatough[16], P.G. Estabrooks[6], E. Etzion[23], H.G. Evans[9], F. Fabbri[2], M. Fanti[2], A.A. Faust[30], F. Fiedler[27], M. Fierro[2], I. Fleck[8], R. Folman[26], A. Fürtjes[8], D.I. Futyan[16], P. Gagnon[7], J.W. Gary[4], J. Gascon[18], S.M. Gascon-Shotkin[17], G. Gaycken[27], C. Geich-Gimbel[3], G. Giacomelli[2], P. Giacomelli[2], V. Gibson[5], W.R. Gibson[13], D.M. Gingrich[30,a], D. Glenzinski[9], J. Goldberg[22], W. Gorn[4], C. Grandi[2], E. Gross[26], J. Grunhaus[23], M. Gruwé[27], G.G. Hanson[12], M. Hansroul[8], M. Hapke[13], K. Harder[27], C.K. Hargrove[7], C. Hartmann[3], M. Hauschild[8], C.M. Hawkes[5], R. Hawkings[27], R.J. Hemingway[6], M. Herndon[17], G. Herten[10], R.D. Heuer[8], M.D. Hildreth[8], J.C. Hill[5], S.J. Hillier[1], P.R. Hobson[25], A. Hocker[9], R.J. Homer[1], A.K. Honma[28,a], D. Horváth[32,c], K.R. Hossain[30], R. Howard[29], P. Hüntemeyer[27], P. Igo-Kemenes[11], D.C. Imrie[25], K. Ishii[24], F.R. Jacob[20], A. Jawahery[17], H. Jeremie[18], M. Jimack[1], C.R. Jones[5], P. Jovanovic[1], T.R. Junk[6], D. Karlen[6], V. Kartvelishvili[16], K. Kawagoe[24], T. Kawamoto[24], P.I. Kayal[30], R.K. Keeler[28], R.G. Kellogg[17], B.W. Kennedy[20], A. Klier[26], S. Kluth[8], T. Kobayashi[24], M. Kobel[3,e], D.S. Koetke[6], T.P. Kokott[3], M. Kolrep[10], S. Komamiya[24], R.V. Kowalewski[28], T. Kress[11], P. Krieger[6], J. von Krogh[11], T. Kuhl[3], P. Kyberd[13], G.D. Lafferty[16], D. Lanske[14], J. Lauber[15], S.R. Lautenschlager[31], I. Lawson[28], J.G. Layter[4], D. Lazic[22], A.M. Lee[31], D. Lellouch[26], J. Letts[12], L. Levinson[26], R. Liebisch[11], B. List[8], C. Littlewood[5], A.W. Lloyd[1], S.L. Lloyd[13], F.K. Loebinger[16], G.D. Long[28], M.J. Losty[7], J. Ludwig[10], D. Liu[12], A. Macchiolo[2], A. Macpherson[30], W. Mader[3], M. Mannelli[8], S. Marcellini[2], C. Markopoulos[13], A.J. Martin[13], J.P. Martin[18], G. Martinez[17], T. Mashimo[24], P. Mättig[26], W.J. McDonald[30], J. McKenna[29], E.A. Mckigney[15], T.J. McMahon[1], R.A. McPherson[28], F. Meijers[8], S. Menke[3], F.S. Merritt[9], H. Mes[7], J. Meyer[27], A. Michelini[2], S. Mihara[24], G. Mikenberg[26], D.J. Miller[15], R. Mir[26], W. Mohr[10], A. Montanari[2], T. Mori[24], K. Nagai[8], I. Nakamura[24], H.A. Neal[12], B. Nellen[3], R. Nisius[8], S.W. O'Neale[1], F.G. Oakham[7], F. Odorici[2], H.O. Ogren[12], M.J. Oreglia[9], S. Orito[24], J. Pálinkás[33,d], G. Pásztor[32], J.R. Pater[16], G.N. Patrick[20], J. Patt[10], R. Perez-Ochoa[8], S. Petzold[27], P. Pfeifenschneider[14], J.E. Pilcher[9], J. Pinfold[30], D.E. Plane[8], P. Poffenberger[28], J. Polok[8], M. Przybycień[8], C. Rembser[8], H. Rick[8], S. Robertson[28], S.A. Robins[22], N. Rodning[30], J.M. Roney[28], K. Roscoe[16], A.M. Rossi[2], Y. Rozen[22], K. Runge[10], O. Runolfsson[8], D.R. Rust[12], K. Sachs[10], T. Saeki[24], O. Sahr[34], W.M. Sang[25], E.K.G. Sarkisyan[23], C. Sbarra[29], A.D. Schaile[34], O. Schaile[34], F. Scharf[3], P. Scharff-Hansen[8], J. Schieck[11], B. Schmitt[8], S. Schmitt[11], A. Schöning[8], M. Schröder[8], M. Schumacher[3], C. Schwick[8], W.G. Scott[20], R. Seuster[14], T.G. Shears[8], B.C. Shen[4], C.H. Shepherd-Themistocleous[8], P. Sherwood[15], G.P. Siroli[2], A. Sittler[27], A. Skuja[17], A.M. Smith[8], G.A. Snow[17], R. Sobie[28], S. Söldner-Rembold[10], M. Sproston[20], A. Stahl[3], K. Stephens[16], J. Steuerer[27], K. Stoll[10], D. Strom[19], R. Ströhmer[34], B. Surrow[8], S.D. Talbot[1], S. Tanaka[24], P. Taras[18], S. Tarem[22], R. Teuscher[8], M. Thiergen[10], M.A. Thomson[8], E. von Törne[3], E. Torrence[8], S. Towers[6], I. Trigger[18], Z. Trócsányi[33], E. Tsur[23], A.S. Turcot[9], M.F. Turner-Watson[8], R. Van Kooten[12], P. Vannerem[10], M. Verzocchi[10], H. Voss[3], F. Wäckerle[10], A. Wagner[27], C.P. Ward[5], D.R. Ward[5], P.M. Watkins[1], A.T. Watson[1], N.K. Watson[1], P.S. Wells[8], N. Wermes[3], J.S. White[6], G.W. Wilson[16], J.A. Wilson[1], T.R. Wyatt[16], S. Yamashita[24], G. Yekutieli[26], V. Zacek[18], D. Zer-Zion[8]

[1]School of Physics and Astronomy, University of Birmingham, Birmingham B15 2TT, UK
[2]Dipartimento di Fisica dell' Università di Bologna and INFN, I-40126 Bologna, Italy
[3]Physikalisches Institut, Universität Bonn, D-53115 Bonn, Germany
[4]Department of Physics, University of California, Riverside CA 92521, USA
[5]Cavendish Laboratory, Cambridge CB3 0HE, UK
[6]Ottawa-Carleton Institute for Physics, Department of Physics, Carleton University, Ottawa, Ontario K1S 5B6, Canada
[7]Centre for Research in Particle Physics, Carleton University, Ottawa, Ontario K1S 5B6, Canada
[8]CERN, European Organisation for Particle Physics, CH-1211 Geneva 23, Switzerland

^{9}Enrico Fermi Institute and Department of Physics, University of Chicago, Chicago IL 60637, USA
^{10}Fakultät für Physik, Albert Ludwigs Universität, D-79104 Freiburg, Germany
^{11}Physikalisches Institut, Universität Heidelberg, D-69120 Heidelberg, Germany
^{12}Indiana University, Department of Physics, Swain Hall West 117, Bloomington IN 47405, USA
^{13}Queen Mary and Westfield College, University of London, London E1 4NS, UK
^{14}Technische Hochschule Aachen, III Physikalisches Institut, Sommerfeldstrasse 26-28, D-52056 Aachen, Germany
^{15}University College London, London WC1E 6BT, UK
^{16}Department of Physics, Schuster Laboratory, The University, Manchester M13 9PL, UK
^{17}Department of Physics, University of Maryland, College Park, MD 20742, USA
^{18}Laboratoire de Physique Nucléaire, Université de Montréal, Montréal, Quebec H3C 3J7, Canada
^{19}University of Oregon, Department of Physics, Eugene OR 97403, USA
^{20}CLRC Rutherford Appleton Laboratory, Chilton, Didcot, Oxfordshire OX11 0QX, UK
^{22}Department of Physics, Technion-Israel Institute of Technology, Haifa 32000, Israel
^{23}Department of Physics and Astronomy, Tel Aviv University, Tel Aviv 69978, Israel
^{24}International Centre for Elementary Particle Physics and Department of Physics, University of Tokyo, Tokyo 113-0033, and Kobe University, Kobe 657-8501, Japan
^{25}Institute of Physical and Environmental Sciences, Brunel University, Uxbridge, Middlesex UB8 3PH, UK
^{26}Particle Physics Department, Weizmann Institute of Science, Rehovot 76100, Israel
^{27}Universität Hamburg/DESY, II Institut für Experimental Physik, Notkestrasse 85, D-22607 Hamburg, Germany
^{28}University of Victoria, Department of Physics, P O Box 3055, Victoria BC V8W 3P6, Canada
^{29}University of British Columbia, Department of Physics, Vancouver BC V6T 1Z1, Canada
^{30}University of Alberta, Department of Physics, Edmonton AB T6G 2J1, Canada
^{31}Duke University, Dept of Physics, Durham, NC 27708-0305, USA
^{32}Research Institute for Particle and Nuclear Physics, H-1525 Budapest, P O Box 49, Hungary
^{33}Institute of Nuclear Research, H-4001 Debrecen, P O Box 51, Hungary
^{34}Ludwigs-Maximilians-Universität München, Sektion Physik, Am Coulombwall 1, D-85748 Garching, Germany

Abstract. The fraction of $Z^0 \to b\bar{b}$ events in hadronic Z^0 decays has been measured by the OPAL experiment using the data collected at LEP between 1992 and 1995. The $Z^0 \to b\bar{b}$ decays were tagged using displaced secondary vertices, and high momentum electrons and muons. Systematic uncertainties were reduced by measuring the b-tagging efficiency using a double tagging technique. Efficiency correlations between opposite hemispheres of an event are small, and are well understood through comparisons between real and simulated data samples. A value of

$$R_b \equiv \frac{\sigma(e^+e^- \to b\bar{b})}{\sigma(e^+e^- \to \text{hadrons})} = 0.2178 \pm 0.0011 \pm 0.0013$$

was obtained, where the first error is statistical and the second systematic. The uncertainty on R_c, the fraction of $Z^0 \to c\bar{c}$ events in hadronic Z^0 decays, is not included in the errors. The dependence on R_c is

$$\frac{\Delta R_b}{R_b} = -0.056 \frac{\Delta R_c}{R_c},$$

where ΔR_c is the deviation of R_c from the value 0.172 predicted by the Standard Model. The result for R_b agrees with the value of 0.2155 ± 0.0003 predicted by the Standard Model.

1 Introduction

The partial width for the decay $Z^0 \rightarrow b\bar{b}$ is of special interest in the Standard Model. Electroweak corrections involving the top quark affect the $Z^0 \rightarrow b\bar{b}$ partial width, $\Gamma_{b\bar{b}}$, differently from the widths for lighter quarks. As a

[a] and at TRIUMF, Vancouver, Canada V6T 2A3
[b] and Royal Society University Research Fellow
[c] and Institute of Nuclear Research, Debrecen, Hungary
[d] and Department of Experimental Physics, Lajos Kossuth University, Debrecen, Hungary
[e] on leave of absence from the University of Freiburg

result, the fraction

$$\frac{\Gamma_{b\bar{b}}}{\Gamma_{\mathrm{had}}} \equiv \frac{\Gamma(Z^0 \rightarrow b\bar{b})}{\Gamma(Z^0 \rightarrow \mathrm{hadrons})}$$

depends on the top quark mass, m_{top}, but has negligible uncertainty from the unknown Higgs boson mass and the strong coupling constant α_s. The fraction $\Gamma_{b\bar{b}}/\Gamma_{\mathrm{had}}$ is also sensitive to various extensions of the Standard Model involving new particles such as additional quarks and gauge bosons, or the virtual effects of new scalars and fermions such as those expected in supersymmetric models [1].

The quantity measured in this analysis is the cross-section ratio

$$R_b \equiv \frac{\sigma(e^+e^- \to b\bar{b})}{\sigma(e^+e^- \to \text{hadrons})}$$

at the Z^0 resonance. This differs from the partial width ratio $\Gamma_{b\bar{b}}/\Gamma_{\text{had}}$ because of the additional contribution from photon-exchange diagrams. These have been evaluated within the Standard Model using the program ZFITTER 5.0 [2] which predicts that R_b is 0.0002 smaller than $\Gamma_{b\bar{b}}/\Gamma_{\text{had}}$. By convention, $Z^0 \to b\bar{b}$ events where an additional $q\bar{q}$ pair is produced via gluon splitting are included in the numerators of the definitions of $\Gamma_{b\bar{b}}/\Gamma_{\text{had}}$ and R_b. The small number of events where the only $b\bar{b}$ pair is produced via gluon splitting, rather than directly from Z^0 decay, is not included in the numerators. The interference between these two processes, and the effect on the measurement of R_b, are expected to be negligible [3].

This paper supersedes the previously published OPAL measurement [4] of the fraction of $b\bar{b}$ events in hadronic Z^0 decays. The measurement is improved by employing higher performance vertex tagging using the upgraded silicon detector with two-coordinate readout installed in 1993 [5], higher performance electron identification, and by including the data taken in 1995.

The paper is organised as follows. The analysis method, based on the double tagging technique, is described in the next section. The OPAL detector, the selected event sample and the Monte Carlo simulation are reviewed in Sect. 3. The b-tagging methods are discussed in Sects. 4 and 5. The result is presented in Sect. 6, with systematic errors being evaluated in Sects. 7 and 8. A summary is given in Sect. 9.

2 Analysis method

The analysis method is based on the double tagging technique. Each selected hadronic Z^0 decay event is divided into two hemispheres by the plane perpendicular to the thrust axis and containing the interaction point. A b-tagging algorithm is then applied separately to each hemisphere, and the number of tagged hemispheres N_t and events where both hemispheres are tagged N_{tt} counted in the sample of N_{had} selected hadronic events. These quantities are related by:

$$N_t = 2N_{\text{had}}\{\epsilon^b \, R_b \, + \epsilon^c \, R_c \, + \epsilon^{\text{uds}} \, (1 - R_b - R_c)\}, \quad (1)$$

$$N_{tt} = N_{\text{had}}\{C^b \, (\epsilon^b)^2 \, R_b + C^c(\epsilon^c)^2 \, R_c$$
$$+ C^{\text{uds}}(\epsilon^{\text{uds}})^2 \, (1 - R_b - R_c)\}, \quad (2)$$

where ϵ^b, ϵ^c and ϵ^{uds} are the tagging efficiencies for hemispheres in $b\bar{b}$, $c\bar{c}$ and light quark (uds) events, and C^b, C^c and C^{uds} describe the tagging efficiency correlation between the two hemispheres in events of each flavour. For a useful b-tagging algorithm, ϵ^b is much larger than ϵ^c and ϵ^{uds}. The correlation C^b is defined by $C^b = \epsilon^{bb}/(\epsilon^b)^2$, where ϵ^{bb} is the efficiency to tag both hemispheres of a $b\bar{b}$

event. Deviations of C^b from unity account for the fact that the tagging in the two hemispheres is not completely independent, there being a small efficiency correlation between them for both physical and instrumental reasons. These correlations are also present in $c\bar{c}$ and light quark events; however their effect on the R_b measurement is less than 10^{-4} because the double tagging efficiencies for these events are very small. The correlations C^c and C^{uds} are therefore set to unity. The values of R_b and ϵ^b can then be obtained by solving (1) and (2), and only the values of ϵ^c, ϵ^{uds} and C^b need to be input from Monte Carlo simulation. This technique avoids the need to input ϵ^b from simulation, which severely limits the precision of single tag measurements of R_b.

In this analysis, two b-tags are used: a secondary vertex tag with very high b-purity, and a high momentum lepton tag with somewhat lower b-purity and efficiency. A hemisphere is taken to be tagged if it is tagged by either one or both of the secondary vertex and lepton tags. As the performance of the tagging algorithms changes significantly between the different years of data taking due to changes in the detector configuration, the equations are solved separately for ϵ^b and R_b for each year. The values of R_b are then combined, taking into account correlated and uncorrelated systematic uncertainties. The charm tagging efficiencies ϵ^c, light quark tagging efficiencies ϵ^{uds} and $b\bar{b}$ correlation coefficient C^b for each year are input from Monte Carlo simulation, and are thus sources of systematic error. The relative sizes of these systematic errors and the statistical error depend on the purity and efficiency of the b-tag, and the tag cut is adjusted to minimise the total resulting error. The only other sources of systematic error are the value of R_c (which is fixed to its Standard Model value), and the hadronic event selection.

3 Data sample and event simulation

The OPAL detector has been described in detail elsewhere [5,6]. Tracking of charged particles is performed by a central detector, consisting of a silicon microvertex detector, a vertex chamber, a jet chamber and z-chambers[1]. The central detector is positioned inside a solenoid, which provides a uniform axial magnetic field of 0.435 T. The silicon microvertex detector consists of two layers of silicon strip detectors; the inner layer covers a polar angle range of $|\cos\theta| < 0.83$ and the outer layer covers $|\cos\theta| < 0.77$. This detector provided ϕ coordinate information in 1992, and was upgraded to provide both ϕ and z coordinate information from 1993. In 1995, a new detector geometry was installed with smaller gaps between the wafers in ϕ, increasing the fraction of tracks with silicon hits from both layers. The vertex chamber is a precision drift chamber which covers the range $|\cos\theta| < 0.95$. The jet

---

[1] A right handed coordinate system is used, with positive z along the e^- beam direction and x pointing towards the centre of the LEP ring. The polar and azimuthal angles are denoted by θ and ϕ, and the origin is taken to be the centre of the detector

chamber is a large-volume drift chamber, 4.0 m long and 3.7 m in diameter, providing both tracking (precise r-ϕ and coarse r-z) and ionisation energy loss (dE/dx) information. The z-chambers provide a precise measurement of the z-coordinate of tracks as they leave the jet chamber in the range $|\cos\theta| < 0.72$. The coil is surrounded by a time-of-flight counter array and a barrel lead-glass electromagnetic calorimeter with a presampler. Including the endcap electromagnetic calorimeters, the lead-glass blocks cover the range $|\cos\theta| < 0.98$. The magnet return yoke is instrumented with streamer tubes and serves as a hadron calorimeter. Outside the hadron calorimeter are muon chambers, which cover 93% of the full solid angle.

The data used for this analysis were collected from e^+e^- collisions at LEP during 1992–1995, with centre-of-mass energies at and around the peak of the Z^0 resonance. Hadronic events were selected by the algorithm used in [4], giving a hadronic Z^0 selection efficiency of $(98.1 \pm 0.5)\%$ and a background of less than 0.1%. The thrust value T and thrust axis polar angle θ_T were then calculated using charged tracks and electromagnetic clusters not associated to any tracks. To ensure a well defined thrust axis direction within the acceptance of the silicon microvertex detector, the thrust value and axis direction were required to satisfy $T > 0.8$ and $|\cos\theta_T| < 0.7$. The complete selection has an efficiency of about 58% for hadronic Z^0 decays, and selected a total of 1 923 240 events in the data. Of these events, 4.9% were recorded below the peak of the Z^0 resonance at a centre-of-mass energy of $E_{cm} = 89.4$ GeV and 7.4% above the peak at $E_{cm} = 93.0$ GeV. Calculations using ZFITTER [2] indicate that these off-peak events change the measured value of R_b by -0.00004, a correction which is -0.02% of the measured value and is not applied to the result presented here.

The event selection is designed to have the same efficiency for each quark flavour. However, $b\bar{b}$ events have a higher average charged particle multiplicity than other flavours, and hence a slightly higher probability of passing the event selection requirement of at least seven charged tracks. Owing to the high mass of the b quark, $b\bar{b}$ events also have a slightly different thrust distribution, but Monte Carlo studies showed this to have a much smaller effect than that from the track multiplicity cut. According to the Monte Carlo, these biases increase the measured value of R_b in the selected event sample by 0.32% of its value. Non-hadronic background (mainly $e^+e^- \to \tau^+\tau^-$ events) constitutes about 0.065% of the selected events, and reduces the measured value of R_b by 0.065%. The combination of these event selection effects increases the measured value of R_b by $(0.25 \pm 0.15)\%$, where the error is due to the uncertainty in the simulation of the track multiplicity distributions and Monte Carlo statistics [4].

Charged tracks and electromagnetic calorimeter clusters with no associated track were combined into jets using a cone algorithm [7] with a cone half angle of $R = 0.55$ rad and a minimum jet energy of 5 GeV. This algorithm, rather than the JADE algorithm employed in [4], increases the fraction of tracks in the jet coming from the b hadron decay, and improves the b-tagging performance.

Monte Carlo simulated events were used for evaluating backgrounds, acceptances for charm and light quark events, and efficiency correlations between the two hemispheres of an event. Hadronic events were simulated with the JETSET 7.4 generator [8], with parameters tuned by OPAL [9]. The fragmentation function of Peterson et al. [10] was used to describe the fragmentation of b and c quarks. The generated events were passed through a program that simulated the response of the OPAL detector [11] and the same reconstruction algorithms as the data. Further detailed studies of the tracking performance in the data were made, and the results were used to tune the simulated tracking performance.

4 Vertex tagging

Hadronic Z^0 decays into b quarks are tagged by reconstructing secondary vertices significantly separated from the primary vertex, taking advantage of the relatively long (~ 1.5 ps) lifetime, high decay charged multiplicity and high mass (~ 5 GeV) of b hadrons[2]. Information characterising these features of b hadron production and decay is combined using an artificial neural network algorithm to produce a single vertex tagging variable for each hemisphere.

4.1 Primary vertex reconstruction

Primary vertices were reconstructed for each event using the algorithm described in [4], but applied separately to each hemisphere of the event. Reconstructing a separate independent primary vertex in each hemisphere avoids an efficiency correlation from sharing a single primary vertex reconstructed using tracks from both hemispheres [12]. The position and uncertainty of the beam spot (e^+e^- collision region) was used as a common constraint in both hemispheres, but its effect on the correlation is small. The beam spot position was measured using charged tracks from many consecutive events, thus following any significant shifts in beam position during a LEP fill [13].

All good tracks in one hemisphere were fitted to a common vertex in three dimensions. The tracks were required to satisfy various requirements to ensure they were well measured, including having at least 20 hits in the jet chamber, a transverse momentum with respect to the beam axis of at least 0.15 GeV and a distance of closest approach to the beam spot in the r-ϕ plane of less than 5 cm. Tracks with a large χ^2 contribution to the primary vertex fit were removed one by one until each remaining track contributed less than 4 to the χ^2. In about 0.7% of the events, no tracks remained after this procedure, in which case the beam spot position was used.

Using the hemisphere primary vertex reconstruction, the primary vertex resolution in Monte Carlo simulated events with the 1994 silicon detector is about $70\,\mu$m in x,

---

[2] The convention $c = 1$ is assumed throughout this paper

15 μm in y (where it is dominated by the beam spot constraint) and 110 μm in z. Using the event primary vertex reconstruction, the resolutions in x, y and z are 50 μm, 15 μm and 80 μm respectively. The poorer primary vertex resolution in the hemisphere reconstruction method leads to a non-b impurity that is about 10 % higher (relative) for a given b-tagging efficiency, but a much reduced hemisphere efficiency correlation and associated systematic error.

4.2 Secondary vertex reconstruction

A three dimensional version of the algorithm described in [4] was used to reconstruct a secondary vertex in each jet. All tracks in the jet with momentum $p > 0.5$ GeV, a distance of closest approach to the hemisphere primary vertex in the r-ϕ plane ('impact parameter') $d_0 < 0.3$ cm, and an impact parameter error $\sigma_{d_0} < 0.1$ cm, were fitted to a common vertex in three dimensions. These track requirements cause the vertex finding algorithm to tend to select the b hadron decay vertex rather than the primary vertex, because of the high decay multiplicity and hard fragmentation of the b quark. Tracks with a large χ^2 contribution to the fit were removed one by one until each track contributed less than 4 to the overall χ^2. At least three tracks were required to remain in the fit for the secondary vertex finding to be considered successful.

The vertex decay length L was calculated as the length of the vector from the primary to the secondary vertex, the vector being constrained to lie along the direction of the jet axis. L was given a positive sign if the secondary vertex was displaced from the primary in the direction of the jet momentum, and a negative sign otherwise. Vertices with $L > 0$ ('forward') were used in the tagging of b hadron decays, and those with $L < 0$ ('backward') were used to reduce the systematics associated with the detector resolution.

4.3 Vertex tagging neural network

Jets containing a vertex with at least three tracks and satisfying $|L/\sigma_L| > 3$ (where σ_L is the estimated error on L, derived from the track error matrices) were considered pre-selected and input to a neural network algorithm [14]. In the Monte Carlo, the efficiency of this pre-selection for b-jets is about 49% and the b-purity is about 76%.

The neural network was used to enhance the b-purity, and has five input nodes, eight hidden nodes and one output node. The first three inputs were derived directly from the reconstructed secondary vertex: the decay length significance L/σ_L, the decay length L, and the number of tracks in the secondary vertex N_s. The fourth input to the network tests the stability of the vertex against mismeasured tracks. The secondary vertex track with the highest impact parameter significance with respect to the primary vertex (d_0/σ_{d_0}) was removed from the secondary vertex, and the secondary vertex fit repeated resulting in

the 'reduced' decay length significance L_R/σ_{L_R}. For genuine b hadron decays, L_R/σ_{L_R} is large, whilst for vertices caused by one high impact parameter mis-measured track (which is removed from the 'reduced' vertex), L_R/σ_{L_R} is small.

The fifth input exploits the high mass of b hadrons compared with charm hadrons, using a method similar to that described in [12]. For each track in the jet, a weight X that it came from a b hadron decay was computed, using a separate artificial neural network trained on $b\bar{b}$ Monte Carlo events. This network has six inputs, eight hidden nodes and one output node. The inputs are: the scaled track momentum $x_p = p/E_{\text{beam}}$; the sine of the angle of the track with respect to the jet axis $\sin\theta_t = p_t/p$; the impact parameter significances of the track with respect to the reconstructed secondary vertex in the r-ϕ $((d_0/\sigma_{d_0})_{\text{sec}})$ and r-z $((z_0/\sigma_{z_0})_{\text{sec}})$ planes; and the impact parameter significances of the track with respect to the hemisphere primary vertex in the r-ϕ $((d_0/\sigma_{d_0})_{\text{prim}})$ and r-z $((z_0/\sigma_{z_0})_{\text{prim}})$ planes. The impact parameters are signed positive if the crossing point of the track and the jet axis is displaced from the vertex in the same direction as the jet momentum, and negative otherwise. The network was trained separately on tracks with no silicon hits, silicon r-ϕ hits only, and both silicon r-ϕ and r-z hits. The output X of this network represents the probability that the track came from b hadron decay rather than fragmentation.

All tracks within a jet were then ordered by decreasing X (*i.e.* most b hadron decay-like tracks first), and the first two were clustered together. Other tracks were added in turn to the cluster, until the invariant mass of the tracks (assuming them to be pions) exceeded the charm hadron mass, taken to be $m_D = 1.9$ GeV. The value X_D of X for the track which caused the cluster invariant mass to exceed m_D was then used as the fifth input for the vertex neural network. For charm hadron decays, X_D is usually small, since tracks from fragmentation have to be included to exceed m_D. In contrast, b hadrons have enough mass that the threshold can usually be exceeded with tracks from the b hadron decay alone, leading to a value of X_D close to one. If the cluster mass did not exceed m_D after all tracks in the jet had been added, X_D was set to zero; this happens more often in charm and light quark jets than in b jets.

4.4 Vertex tag definition

Samples of five-flavour Monte Carlo jets passing the pre-selection and with $L > 0$ were used to train the main neural network (with inputs L/σ_L, L, N_s, L_R/σ_{L_R} and X_D), to produce output distributions peaking close to zero for light flavour and charm jets, and outputs close to one for b jets.

In order to reduce sensitivity to the modelling of the detector resolution, the technique of 'folding', *i.e.* subtracting the number of hemispheres tagged with negative L, was employed [4]. This technique works well if the tagging variable (in this case the vertex tag neural network
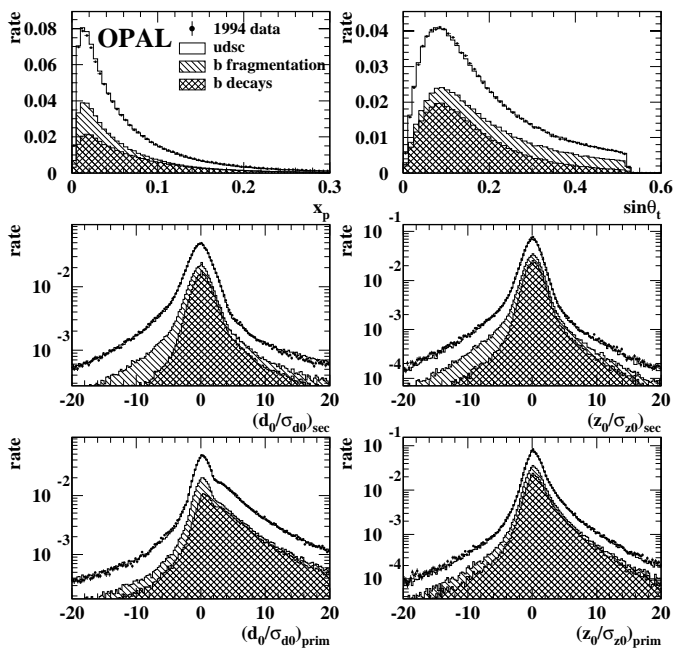
Fig. 1. Distributions of the track neural network input variables x_p, $\sin\theta_t$, $(d_0/\sigma_{d_0})_{\text{sec}}$, $(z_0/\sigma_{z_0})_{\text{sec}}$, $(d_0/\sigma_{d_0})_{\text{prim}}$ and $(z_0/\sigma_{z_0})_{\text{prim}}$ used to derive X_D. The sum of the distributions for the three track classes (no silicon hits, silicon r-ϕ hits only, and both silicon r-ϕ and r-z hits) are shown for 1994 data (points) and 1994 Monte Carlo simulation (histograms). The estimated contribution of tracks from b decay, b fragmentation, and charm and light quark background are indicated

Fig. 2. Distributions of the vertex tagging neural network inputs L/σ_L, L, L_R/σ_{L_R}, N_s and X_D for 1994 data (points) and 1994 Monte Carlo simulation (histogram). The contributions from uds, c and b jets are indicated

output) is symmetric about zero for jets containing no particles with detectable lifetime. To achieve this symmetry, the variables L/σ_L, L and L_R/σ_{L_R} were modified before being input to the neural network. For L/σ_L and L, the absolute values $|L/\sigma_L|$ and $|L|$ were taken, while L_R/σ_{L_R} was signed positive if it originally had the same sign as L, and negative otherwise. The impact parameter significances used to calculate X_D also had their signs reversed if L was negative. The magnitude of the vertex tagging variable B was then defined as $|B| = -\ln(1-b)$ where b is the raw neural network output (between zero and one), and the sign of B was taken to be the sign of L. The logarithmic transformation is just used to expand the scale of the tagging variable in the region just below $b = 1$, and has no effect on the degree of symmetry of the tag distribution.

The use of folding also requires that (1) and (2) are modified appropriately. The tagging efficiencies ϵ are replaced by the difference of forward and backward tagging efficiencies $\epsilon_v - \epsilon_{\overline{v}}$. The number of tagged hemispheres N_t is replaced by the difference between the numbers of forward and backward tagged hemispheres $N_v - N_{\overline{v}}$, and the number of double tagged events N_{tt} is replaced by $N_{vv} - N_{v\overline{v}} + N_{\overline{v}\,\overline{v}}$ where N_{vv}, $N_{v\overline{v}}$ and $N_{\overline{v}\,\overline{v}}$ are the numbers of events with two forward tags, one forward and one backward tag, and two backward tags respectively [4].

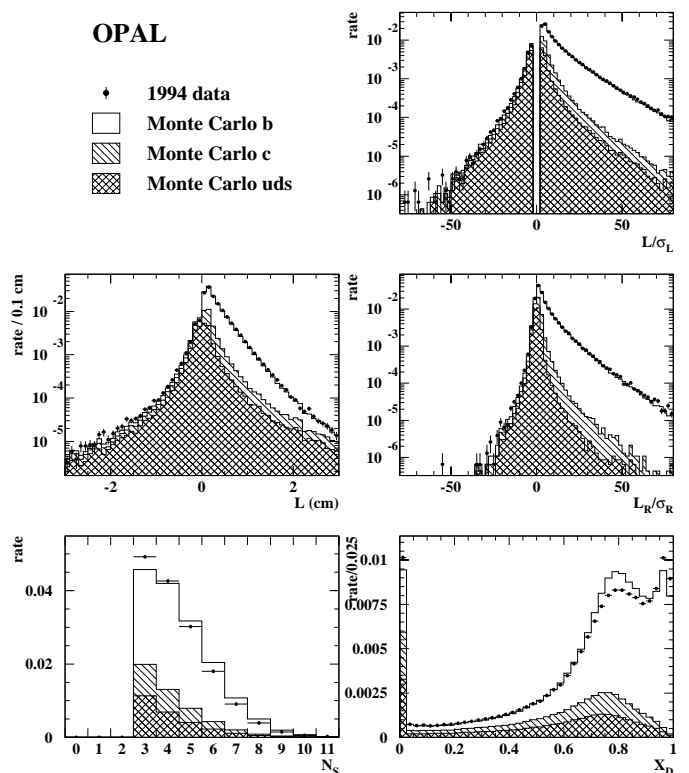As the silicon detector did not provide r-z information in 1992, a separate version of the vertex tagging algorithm was used for these data. Primary and secondary vertices were reconstructed in the r-ϕ plane only, and the r-z impact parameter significances were not used in the calculation of X_D. According to the Monte Carlo, the tagging impurity for 1992 data using the r-ϕ only tagging algorithm is about 30 % higher than that for 1994 data at the same b-tagging efficiency.

4.5 Vertex tag performance

The distributions of the input variables for the track neural network used to derive X_D are shown in Fig. 1, and the distributions of the vertex tag neural network input variables are shown in Fig. 2, for 1994 data and Monte Carlo simulation. In general the modelling of the input variables is good, but some discrepancies are visible, particularly in the distributions of N_s and X_D. These are attributed to imperfections in the detector modelling and in the simulation of b hadron decays. The effects of the former are addressed in the systematic errors, whilst the latter have no impact on the result since the b-tagging efficiency is determined from the data and not from the Monte Carlo.

The distribution of the vertex tagging variable B is shown for 1994 data and Monte Carlo in Fig. 3. Good qualitative agreement is seen. The Monte Carlo distribution for uds jets is seen to be approximately symmetric about $B = 0$, as required for the folding procedure to work well.
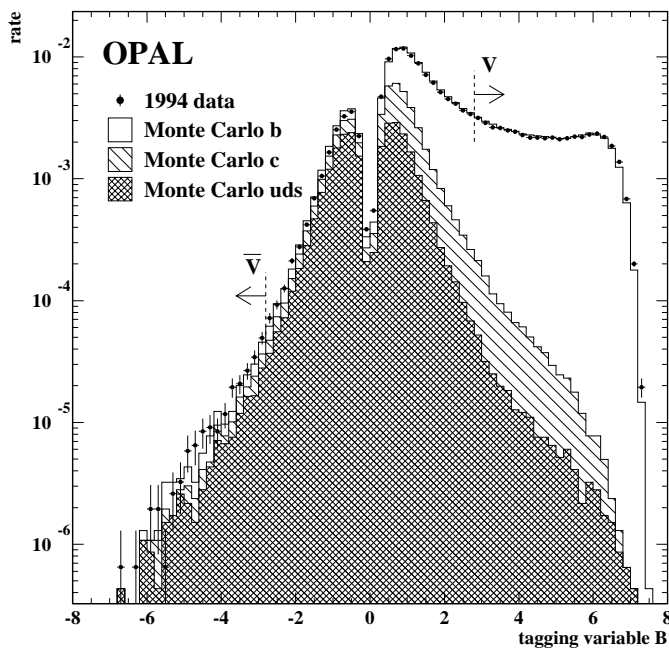
Fig. 3. Distributions of the vertex tagging variable B for the 1994 data (points) and 1994 Monte Carlo simulation (histogram). The positions of the forward and backward tag cuts are shown by dashed lines. The contributions from uds, c and b jets are indicated

The asymmetry in the uds distribution is caused by jets containing a long-lived strange particle (K_S^0, Λ or other hyperon) and by uds jets containing a gluon splitting to a $b\bar{b}$ or $c\bar{c}$ pair. The distributions for charm and especially for b jets are shifted to large positive values of B, and at high values the b jet purity exceeds 99 %.

The hemisphere vertex tag was defined from the vertex tag of any jet in the hemisphere. If more than one jet in the hemisphere passed the vertex tag preselection, the one with the highest value of $|B|$ was used. A hemisphere was then defined to be forward tagged with the vertex tag V if $B > 2.8$ and backward tagged ($\overline{V}$) if $B < -2.8$. The value of 2.8 was chosen to minimise the overall error on R_b when also including the lepton tag.

5 Lepton tagging

Leptons with high momentum p, and a large momentum component transverse to the jet axis p_t, are expected to come mainly from semileptonic decays of b hadrons, because of the hard fragmentation and high mass of the b quark. Electron candidates with $p > 2\,\text{GeV}$ and $p_t > 1.1\,\text{GeV}$, and muon candidates with $p > 3\,\text{GeV}$ and $p_t > 1.4\,\text{GeV}$, were used to tag $b\bar{b}$ events. Both electrons and muons were restricted to the polar angle range $|\cos\theta| < 0.8$ (with respect to the beam axis) to ensure a well-defined acceptance and good Monte Carlo modelling of the efficiencies and backgrounds.

The sources of lepton candidates are divided into two classes. The first class consists of prompt leptons from the decays of b and c hadrons (including $b \rightarrow \tau \rightarrow \ell$ and $b \rightarrow J/\psi \rightarrow \ell$ and those from b and c hadrons produced in gluon splitting). These leptons are included in the definitions of ϵ^b, ϵ^c and ϵ^{uds} for the lepton tag. Monte Carlo is used to estimate ϵ^c and ϵ^{uds}, whereas ϵ^b is determined from the data. The second class of lepton candidates consists of everything else: real leptons produced from Dalitz decays, photon conversions and the decays in flight of $K^\pm$ and $\pi^\pm$, and hadrons mis-identified as leptons. This background is estimated using a combination of data and Monte Carlo, and is subtracted from the number of identified lepton candidates before input to the fit for R_b. These lepton candidates are therefore not included in the definitions of ϵ^b, ϵ^c and ϵ^{uds}.

5.1 Electron identification

Electrons were identified using an artificial neural network. The algorithm is a simplified version of that described in [15], using only six rather than twelve neural network inputs. The inputs are: the momentum and polar angle of the track, the energy-momentum ratio E/p, the number of electromagnetic calorimeter blocks contributing to the energy measurement, the normalised ionisation energy loss $N^\sigma_{dE/dx}$ and the error on the ionisation energy loss $\sigma_{dE/dx}$. The normalised dE/dx value is defined as $N^\sigma_{dE/dx} = (dE/dx - (dE/dx)_0)/(\sigma_{dE/dx})_0$, where $(dE/dx)_0$ is the value and $(\sigma_{dE/dx})_0$ the error expected for the track, assuming it to be an electron of the measured track momentum. The neural network output for electron candidates in data and Monte Carlo is shown in Fig. 4a. Electron candidates were required to have a neural network output greater than 0.95.

Photon conversion candidates were rejected using another neural network algorithm, using spatial matching, invariant mass and momentum information of the electron candidate and an oppositely charged partner track. This algorithm is similar to that described in [15], but uses the new electron neural network algorithm described above. The distributions of this neural network output are shown in Fig. 4b. Electron candidates were required to have a conversion tagging neural network output smaller than 0.5. After all these requirements, the expected identification efficiency for electrons from decays of b hadrons within the kinematic and geometrical acceptance is about 68 %.

The non-prompt background in the tagged electron sample consists of hadrons mis-identified as electrons, untagged photon conversions and a small number of electrons from Dalitz decays of light mesons. The background mis-identification probabilities were found to depend strongly on the p and p_t of the track, but were otherwise largely independent of the event flavour. Since the track p and p_t distributions are different in bottom, charm and light quark events, the number of fake leptons in hemispheres opposite to tagged and untagged hemispheres are different. Therefore, the Monte Carlo was used to determine the fake probability per track as a function of p and p_t. The probabilities were combined with the two dimensional

Table 1. Numbers of hadronic events, tagged hemispheres and double tagged events selected in each year of the data. Background has been subtracted from the lepton samples, and the resulting counts are quoted to the nearest whole number

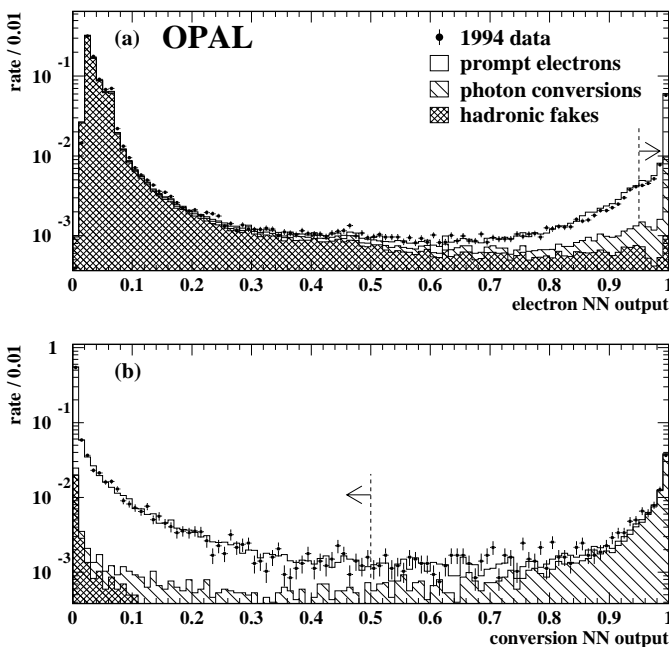|		1992	1993	1994	1995
Number of events	N_{had}	373462	401674	770366	377738
Tagged hemispheres	$N_{\mathrm{v}} - N_{\overline{\mathrm{v}}}$	31455	35942	71624	36248
	N_{ℓ}	7726	8798	16901	8498
	$N_{\mathrm{a}} - N_{\overline{\mathrm{v}}}$	37877	43086	85145	43069
Double tagged events	$N_{\mathrm{vv}} - N_{\mathrm{v\overline{v}}} + N_{\overline{\mathrm{vv}}}$	2934	3562	7376	3964
	$N_{\ell\ell}$	161	171	379	191
	$N_{\mathrm{v}\ell} - N_{\overline{\mathrm{v}}\ell}$	1123	1329	2496	1289
	$N_{\mathrm{aa}} - N_{\mathrm{a}\overline{\mathrm{v}}} + N_{\overline{\mathrm{vv}}}$	4162	4993	10101	5369

Fig. 4a,b. Performance of neural network electron identification in data and Monte Carlo: **a** Normalised distributions of electron neural network output N_{el} for all tracks with $N_{\mathrm{d}E/\mathrm{d}x}^{\sigma} > -2$, $p > 2\,\mathrm{GeV}$ and $p_t > 1.1\,\mathrm{GeV}$; **b** Normalised distributions of the photon conversion tagging neural network output for identified electron tracks with $N_{\mathrm{el}} > 0.95$. In each case, the 1994 data is shown by the points with error bars, and the Monte Carlo contributions from prompt electrons, photon conversions and mis-identified hadrons by the histograms. The selected regions are shown by the dashed lines and arrows

distributions of track p and p_t measured opposite to untagged and tagged (with vertex or lepton) hemispheres in the data, to estimate the number of fake electrons expected opposite to each type of hemisphere. These estimates were then subtracted from the number of lepton tagged hemispheres and events before input to the fit for R_{b}.

In total, 26185 hemispheres were tagged by electrons after the photon conversion rejection. Of these, 918 ± 30 were attributed to hadronic fakes, 784 ± 28 to untagged photon conversions and 210 ± 14 to Dalitz decays of light

mesons, where the background rates have been evaluated by subdividing the fake probabilities by source as a function of p and p_t. The errors are due to data statistics only.

5.2 Muon identification

Muon candidates were identified by matching track segments reconstructed in the four-layer external muon chambers to tracks extrapolated from the central tracking detectors. The measured $\mathrm{d}E/\mathrm{d}x$ was also required to be consistent with a muon. The algorithm is described in detail in [16]. The expected identification efficiency for muons from decays of b hadrons within the kinematic and geometrical acceptance is about 79%.

The muon background was estimated from the Monte Carlo using the same techniques as described in Sect. 5.1. In total, 21558 hemispheres containing muon candidates were found in the data, of which 3311 ± 58 were attributed to hadronic background. The errors are due to data statistics only.

6 Measurement of R_{b}

The numbers of hadronic events, tagged hemispheres and double tagged events found in each year of the data are listed in Table 1. The symbol N_i represents the number of hemispheres tagged by tag i, where $i = \mathrm{v}$ for forward tagged vertices, $i = \overline{\mathrm{v}}$ for backward vertices, $i = \ell$ for leptons and $i = \mathrm{a}$ for hemispheres tagged by either a forward vertex or a lepton. The symbol N_{ij} represents the number of events tagged by tag i in one hemisphere and tag j in the other hemisphere. The expected photon conversion and hadronic backgrounds have already been subtracted from the lepton counts as described in Sect. 5.

The hemisphere tagging probabilities for charm and light quark events, estimated using Monte Carlo simulation, are given in Table 2. The tag probabilities vary slightly from year to year because of the differences in silicon geometrical acceptance and the r-ϕ only tag used in 1992. The Monte Carlo predicted no significant difference in tagging efficiency between $u\overline{u}$, $d\overline{d}$ and $s\overline{s}$ events,

Table 2. Hemisphere tagging probabilities for charm and light quark events estimated from the Monte Carlo for each year of the data. Backward tags have been subtracted from the vertex and combined tag efficiencies. The errors are due to Monte Carlo statistics only

Tag	Year	$c\bar{c}$ (%)	$u\bar{u} + d\bar{d} + s\bar{s}$ (%)
Vertex	1992	0.463 ± 0.009	0.0279 ± 0.0034
	1993	0.457 ± 0.015	0.0256 ± 0.0020
	1994	0.473 ± 0.007	0.0256 ± 0.0014
	1995	0.491 ± 0.009	0.0253 ± 0.0023
Lepton	1992	0.425 ± 0.009	0.0181 ± 0.0016
	1993	0.455 ± 0.013	0.0196 ± 0.0010
	1994	0.443 ± 0.006	0.0172 ± 0.0006
	1995	0.445 ± 0.008	0.0155 ± 0.0010
Combined	1992	0.890 ± 0.013	0.0467 ± 0.0037
	1993	0.902 ± 0.016	0.0425 ± 0.0030
	1994	0.918 ± 0.009	0.0425 ± 0.0015
	1995	0.936 ± 0.012	0.0405 ± 0.0025

Table 3. Hemisphere efficiency correlations in $b\bar{b}$ events estimated from the Monte Carlo with small corrections for each year of the data. The errors are due to Monte Carlo and data statistics only

$C^{\rm b} - 1$ (%)	Vertex	Lepton	Combined
1992	0.84 ± 0.24	1.82 ± 1.29	1.01 ± 0.21
1993	1.10 ± 0.26	1.34 ± 1.28	1.13 ± 0.20
1994	0.77 ± 0.22	1.13 ± 1.25	0.92 ± 0.18
1995	0.99 ± 0.24	0.92 ± 1.28	0.95 ± 0.19

and the effect on $R_{\rm b}$ of assuming a common efficiency was estimated to be less than 10^{-6}.

The $b\bar{b}$ tagging efficiency correlations $C^{\rm b} - 1$ for each year of the data are listed in Table 3. These values were determined from a Monte Carlo sample of 7 million $b\bar{b}$ events, by calculating the ratio of the event double tagging probability to the product of the hemisphere single tagging probabilities. Small corrections for the differing detector performance in each year were derived from the data, as will be discussed in Sect. 8.5. The errors include contributions from the Monte Carlo and data statistics only.

The values of $R_{\rm b}$ and the tagging efficiencies $\epsilon^{\rm b}$ derived for each year of the data are given in Table 4. The results are obtained by solving (1) and (2). The full result from the combined tag is calculated using the number of tagged hemispheres $N_{\rm a} - N_{\bar{\rm v}}$ and the number of double tagged events $N_{\rm aa} - N_{\rm a\bar{v}} + N_{\bar{\rm v}\bar{\rm v}}$. Results are also given for the vertex tag alone ($N_{\rm v} - N_{\bar{\rm v}}$ and $N_{\rm vv} - N_{\rm v\bar{v}} + N_{\bar{\rm v}\bar{\rm v}}$) and the lepton tag alone (N_{ℓ} and $N_{\ell\ell}$). The results have been corrected for the event selection bias described in Sect. 3. Only the data statistical errors are included. The results from the combined tag for the four years agree with each other at a χ^2 of 1.8 for 3 degrees of freedom; the corresponding values of χ^2 for the vertex and lepton tags alone are 3.4 and 2.9 respectively. Combining the data from all

four years, the value of $R_{\rm b}$ is measured to be:

$$R_{\rm b} = 0.2178 \pm 0.0011$$

where the error is due to the data statistics only.

The result depends on $R_{\rm c}$ as follows:

$$\frac{\Delta R_{\rm b}}{R_{\rm b}} = -0.056 \frac{\Delta R_{\rm c}}{R_{\rm c}}$$

where $\Delta R_{\rm c}$ is the deviation of $R_{\rm c}$ from the value 0.172 predicted by the Standard Model and used in this analysis.

The systematic errors coming from sources other than $R_{\rm c}$ are discussed below and are summarised in Table 5. Most of the systematic errors arise through the charm and light quark hemisphere tagging efficiencies, $\epsilon^{\rm c}$ and $\epsilon^{\rm uds}$, and through the $b\bar{b}$ tagging efficiency correlation $C^{\rm b}$. The dependence of $R_{\rm b}$ on these quantities is given approximately by:

$$\frac{\Delta R_{\rm b}}{R_{\rm b}} = -0.059 \frac{\Delta \epsilon^{\rm c}}{\epsilon^{\rm c}} - 0.010 \frac{\Delta \epsilon^{\rm uds}}{\epsilon^{\rm uds}} + \frac{\Delta C^{\rm b}}{C^{\rm b}} \qquad (3)$$

The systematic errors arising from the charm and light quark efficiencies are discussed in detail in Sect. 7, and those from the efficiency correlation in Sect. 8. The systematic errors on the efficiencies are also given in Table 5. The only other source of systematic error is the hadronic event selection, which was discussed in Sect. 3 and gives rise to an error of ± 0.00033 on $R_{\rm b}$.

As a cross check, the cut on the vertex tag neural network output B was varied in the range 2.2–3.8, and the cuts on the lepton transverse momenta were varied by up to $\pm 0.3\,{\rm GeV}$ from their nominal values. The values of $R_{\rm b}$ obtained are shown in Fig. 5, together with the uncorrelated parts of the statistical and systematic errors. No significant trend in the measured value of $R_{\rm b}$ is observed within these errors.

7 Systematic errors: tagging efficiencies

Systematic errors on the tagging efficiencies $\epsilon^{\rm c}$ and $\epsilon^{\rm uds}$ arise from the understanding of the tracking detectors, the electron and muon identification, and the various physics parameters input to the Monte Carlo simulation.

7.1 Tracking detector performance

The evaluation of the charm and light quark tagging efficiencies for the vertex tag requires an accurate simulation of the detector resolution for charged tracks. The Monte Carlo simulation has been tuned to reproduce the tracking resolution seen in each year of the data by studying the negative impact parameter distributions of tracks (which are sensitive to the resolution), as functions of track momentum, polar angle and the different sub-detectors contributing hits. After tuning, the distributions agree well, as can be seen in Fig. 1. The folding technique used in the vertex tag (see Sect. 4.4) makes the result of this analysis

Table 4. Values of R_{b} and ϵ^{b} measured in each year of the data, after correlation and event selection bias correction. Only statistical errors are included

		Vertex	Lepton	Combined
R_{b}	1992	0.2169 ± 0.0033	0.2156 ± 0.0174	0.2164 ± 0.0027
	1993	0.2182 ± 0.0030	0.2495 ± 0.0199	0.2182 ± 0.0025
	1994	0.2176 ± 0.0021	0.2113 ± 0.0110	0.2194 ± 0.0018
	1995	0.2120 ± 0.0027	0.2171 ± 0.0160	0.2157 ± 0.0023
	Combined	0.2163 ± 0.0013	0.2184 ± 0.0074	0.2178 ± 0.0011
ϵ^{b}	1992	0.1893 ± 0.0030	0.0439 ± 0.0035	0.2254 ± 0.0029
	1993	0.2002 ± 0.0029	0.0406 ± 0.0032	0.2369 ± 0.0028
	1994	0.2087 ± 0.0021	0.0477 ± 0.0025	0.2429 ± 0.0020
	1995	0.2211 ± 0.0030	0.0477 ± 0.0035	0.2550 ± 0.0028

Table 5. Systematic errors on the measured value of R_{b}. The uncertainties on the charm and light quark efficiencies are also given. The systematic errors arising from the efficiencies and lepton identification background are discussed in Sect. 7, those from efficiency correlation in Sect. 8 and that from the event selection in Sect. 3

Source	$\Delta\epsilon^{\mathrm{c}}/\epsilon^{\mathrm{c}}$ (%)	$\Delta\epsilon^{\mathrm{uds}}/\epsilon^{\mathrm{uds}}$ (%)	ΔR_{b}
Tracking resolution	1.24	4.0	0.00017
Tracking efficiency	0.80	4.0	0.00014
Silicon hit matching efficiency	0.82	2.8	0.00009
Silicon alignment	0.58	2.1	0.00008
Electron identification efficiency	1.11	0.5	0.00015
Muon identification efficiency	0.64	0.2	0.00009
c quark fragmentation	2.26	-	0.00028
c hadron production fractions	3.66	-	0.00046
c hadron lifetimes	0.55	-	0.00007
c charged decay multiplicity	1.09	-	0.00014
c neutral decay multiplicity	2.39	-	0.00030
Branching fraction $B(\mathrm{D} \to \mathrm{K}^0)$	1.20	-	0.00015
c semileptonic branching fraction	2.44	-	0.00031
c semileptonic decay modelling	2.34	-	0.00029
Gluon splitting to $\mathrm{c\bar{c}}$	0.34	6.3	0.00018
Gluon splitting to $\mathrm{b\bar{b}}$	0.50	9.3	0.00027
K^0 and hyperon production	-	0.3	0.00001
Monte Carlo statistics (c, uds)	0.66	2.5	0.00010
Subtotal $\Delta\epsilon^{\mathrm{c}}$ and $\Delta\epsilon^{\mathrm{uds}}$	6.65	13.3	0.00090
Electron identification background			0.00039
Muon identification background			0.00041
Efficiency correlation ΔC^{b}			0.00066
Event selection bias			0.00033
Total			0.00129

rather insensitive to the details of the tuning procedure and the applied corrections.

The effect of uncertainties in this procedure was evaluated as follows:

Tracking resolution: The sensitivity to the tracking resolution was assessed by degrading or improving the resolution in the Monte Carlo. This was done by ap-

plying a single multiplicative scale factor β to the difference between the reconstructed and true track parameters of all charged tracks [4]. A $\pm 10\%$ variation was applied to the r-ϕ track parameters (the impact parameter d_0 and track azimuthal angle ϕ_0). An independent $\pm 10\%$ variation was applied to the analogous parameters in the r-z plane. Together with uncertainties in the simulation of b hadron decays and
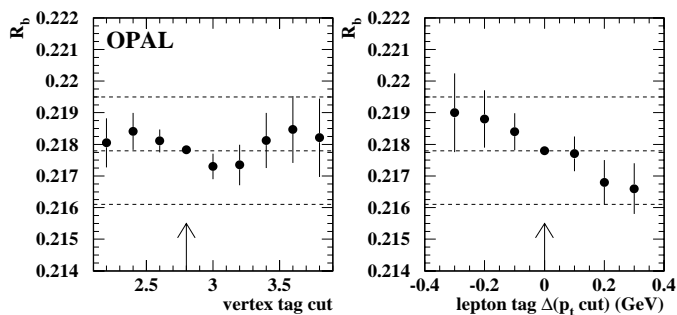
Fig. 5. Values of R_{b} obtained at different cut values. The central value is indicated by the arrow and the dashed lines indicate the total statistical and systematic error. The error bars indicate the uncertainties on the differences from the central result, including both statistical and systematic components

Fig. 6. Forward (f_{v}), backward ($f_{\overline{\mathrm{v}}}$) and folded ($f_{\mathrm{v}} - f_{\overline{\mathrm{v}}}$) hemisphere tagging fractions in each year for the vertex tag. The data tagging rates are shown by the shaded bars, the width of the bars representing the statistical error. The Monte Carlo predictions as a function of the r-ϕ resolution scaling parameter $\beta_{r\phi}$ are shown by the points with error bars

fragmentation, these variations can account for all the discrepancies observed between data and Monte Carlo in the neural network input and output distributions. The result of these variations is an error of ±0.00017 on R_{b}.

The sensitivity to the tails of the impact parameter distribution was also checked, by randomly smearing 2% of the track impact parameters by 15 times their measurement error. This variation (which is much larger than the discrepancies seen in Fig. 1) produced no significant effect in the folded tag efficiencies.

Track reconstruction efficiency: The reconstruction efficiency for charged tracks is estimated to exceed 98% for the momentum and impact parameter requirements described in Sects. 4.1 and 4.2. Most of the losses occur in small regions of ϕ around the jet chamber cathode and anode wire planes. The ϕ distribution of reconstructed tracks is well reproduced by the Monte Carlo simulation, as is the two-track resolution and the rate of tracks lost because they lie on top of another track when reflected in the anode plane. Residual discrepancies indicate that the track reconstruction efficiency is modelled to within $\pm1\%$. The effect on R_{b} was assessed by randomly discarding 1% of tracks in the Monte Carlo, and was found to be ±0.00014.

Silicon hit association efficiency: The Monte Carlo was tuned to model the overall rate of associating silicon hits to tracks, and to model known inefficient regions of the silicon detector in the 1993 and 1994 data. The residual discrepancies between data and Monte Carlo association efficiencies were found to be within $\pm1\%$ for the r-ϕ and $\pm3\%$ for the r-z hits. The hit association efficiency in the Monte Carlo was varied within these errors resulting in a systematic error on R_{b} of ±0.00009.

Silicon alignment: The position of the r-ϕ silicon wafers in the azimuthal direction, and the r-z wafers along the z direction, is determined by an alignment procedure using $\mathrm{Z}^0 \rightarrow \mu^+\mu^-$ events to a precision of about $10\,\mu\mathrm{m}$ [6]. This uncertainty is included in the Monte Carlo simulation, but has little impact on the track resolution in hadronic events which is dominated
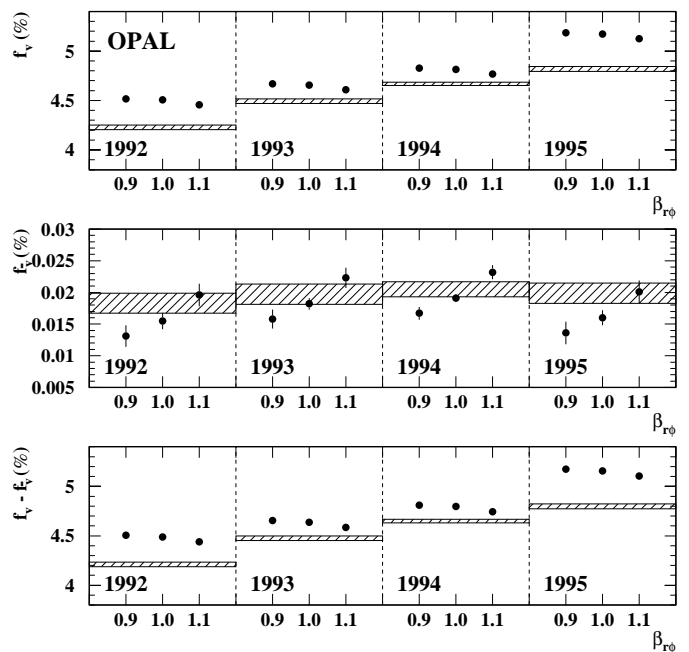
by multiple scattering. The radial alignment uncertainty is much more important since radial shifts of individual wafers can lead to systematic mis-measurement of the decay length L in jets contained largely within a single wafer. The radial alignment was studied using cosmic rays (which are incident on the wafers at all angles) recorded throughout the data taking period and found to be good to a precision of $\pm20\,\mu\mathrm{m}$. The effect on the tagging efficiencies was studied by systematically displacing one or both silicon barrels radially by $20\,\mu\mathrm{m}$ in the simulation, and was found to correspond to an error of ±0.00008 on R_{b}.

The forward, backward and folded vertex tagging rates measured in each year of the data are shown in Fig. 6. The Monte Carlo prediction as a function of the r-ϕ resolution parameter β is also shown. The Monte Carlo forward tagging rate is not important, since the b-tagging efficiency is determined directly from the data using the double tagging technique. It is always somewhat higher in the Monte Carlo than in the data, but the observed discrepancies are within the uncertainties associated with b-physics and detector simulation in the Monte Carlo. The changes in tagging rates as a function of year are mainly caused by differences in the silicon detector in each year of data taking. In 1992, only r-ϕ coordinate information was available, the r-z wafers being installed before the 1993 run [5]. A faulty silicon module in 1993 was replaced for the 1994 run, and a new detector with increased coverage installed for 1995.

The Monte Carlo simulation has been tuned by studying the impact parameter distributions of single tracks. This procedure is not sensitive to possible coherent effects affecting all the tracks in a small number of jets in a correlated way. For example, such effects can be caused by a badly mis-reconstructed primary vertex, which could change the impact parameters of all tracks in a jet, potentially giving an apparent large negative decay length and hence a backward tag. However, the discrepancies in the backward tagging rates seen in Fig. 6 are within the range covered by the $\pm 10\,\%$ variation in the r-ϕ resolution parameter β, so such coherent tracking resolution effects are not likely to be important. This was also checked by studying tails in the distributions of differences in the primary vertex position measured in each hemisphere.

The effect of the r-ϕ resolution scaling on the light quark and charm tagging efficiencies is shown in Fig. 7, for variations in $\beta_{r\phi}$ between 0.8 and 1.2 ($\pm 20\,\%$). These variations cause large changes in the light quark (uds) forward and backward tagging efficiencies, but these changes largely cancel in the folded tagging efficiencies, thus reducing the systematic uncertainty. In contrast, the charm tagging efficiency is dominated by real lifetime tags, and the folding procedure has only a small effect.

7.2 Electron identification

Monte Carlo simulation was used to predict the efficiency for identifying prompt electrons from c $\rightarrow$ e decays and those from gluon splitting g $\rightarrow$ (b$\bar{\text{b}}$, c$\bar{\text{c}}$) $\rightarrow$ e, and background rates as function of track p and p_t. The modelling of the electron identification requirements in the Monte Carlo was checked by studying in detail the distributions of the input variables of the neural network, both for all tracks and in various control samples. The effects on the electron identification performance of discrepancies due to each input variable were added in quadrature to estimate the total systematic errors. This procedure was cross checked with samples of electrons and hadrons selected from various pure control samples.

The Monte Carlo efficiency prediction was checked by studying the neural network input distributions and with samples of pure electrons from e$^+$e$^-$ $\rightarrow$ e$^+$e$^-$ events and photon conversions, and was found to be modelled to a relative precision of $\pm 4\,\%$. According to the Monte Carlo, about 2.6\,% of true prompt electrons are rejected by the photon conversion finder, and this was checked to a relative precision of $\pm 30\,\%$ by comparing samples of high p and p_t electrons in the data and Monte Carlo. This corresponds to a further error of $\pm 0.8\,\%$ on the prompt electron efficiency. Combining both the electron identification and photon rejection uncertainties gives a systematic error on R_b of ± 0.00015.

The two main non-prompt backgrounds in the tagged electron sample are charged hadrons (mainly $\pi^\pm$) which are mis-identified as electrons, and untagged photon conversions. The effect of mis-modelling of the neural network input distributions in the Monte Carlo was found to correspond to an uncertainty of $\pm 21\,\%$ in the hadron mis-
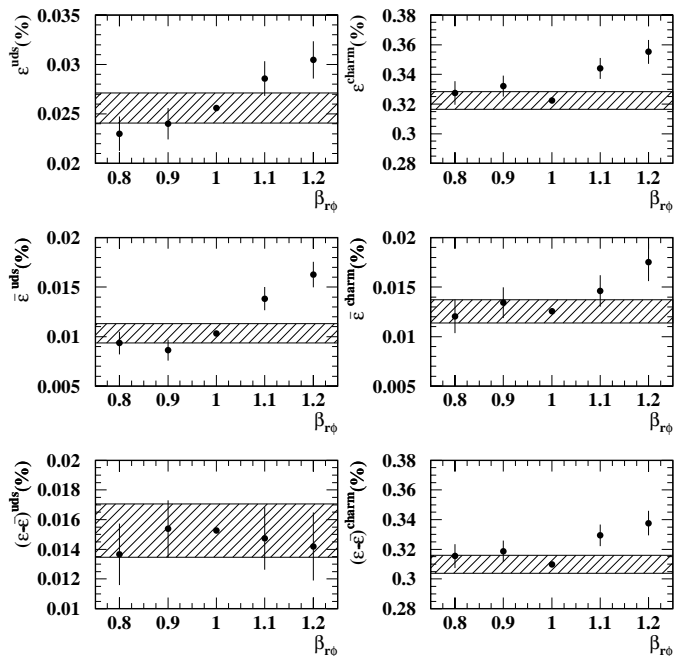

Fig. 7. Forward (ϵ), backward ($\bar{\epsilon}$) and folded ($\epsilon - \bar{\epsilon}$) vertex tagging efficiencies, and their differences for light quark (uds) and charm hemispheres in 1994 Monte Carlo, as a function of the r-ϕ resolution scaling parameter $\beta_{r\phi}$. The shaded bands around the central $\beta_{r\phi} = 1.0$ points show the total statistical error, and the error bars on the other points show the statistical errors on the difference between them and the central points

identification probability. Consistent results were found using control samples of $\pi^\pm$ selected in $K_s^0 \rightarrow \pi^+\pi^-$ and $\tau \rightarrow 3\pi$ decays. The probability for mis-identified hadrons to pass the conversion rejection requirements was found to be modelled to $\pm 5\,\%$ using the $K_s^0 \rightarrow \pi^+\pi^-$ sample, a sample of prompt muons (which have similar p and p_t distributions to prompt electrons and no photon conversion background) and an inclusive electron-depleted sample selected using an anti-cut on the electron identification neural network.

The untagged photon conversion background was studied using a sample of identified electrons, enriched in conversions by requiring the tracks to have low p and p_t. The number of untagged conversions was found to be modelled to a precision of $\pm 15\,\%$. A small number of electrons are also produced in the Dalitz decay of π^0 and η mesons. The Monte Carlo prediction was used for this rate, and a $\pm 20\,\%$ uncertainty used to assess the systematic error, based on measurements of inclusive π^0 and η production in hadronic events [17]. The total systematic error on R_b from all the background sources was found to be ± 0.00039.

7.3 Muon identification

The muon identification efficiency was studied using various control samples in data and Monte Carlo [16]. The muon matching requirements were studied using muon pairs from two-photon production, for muons in the range

2 to 6 GeV, and muon pairs from $Z^0 \to \mu^+\mu^-$ events for muons above 30 GeV. The efficiency of the dE/dx requirement was studied using $K_s^0 \to \pi^+\pi^-$ decays. The Monte Carlo was found to model the matching and dE/dx requirement efficiencies to relative precisions of 2.1 % and 2.2 % respectively, to give a total error on the muon identification efficiency of 3 %. This corresponds to an error of ± 0.00009 on R_b.

The various sources of background muons were studied using control samples from $K_s^0 \to \pi^+\pi^-$ and $\tau \to 3\pi$ decays, and by studying muon candidates failing the dE/dx cut, as in [16]. The background in the data was found to be a factor 1.13 ± 0.09 higher than that in the Monte Carlo, and the fake probabilities per track were corrected accordingly. The resulting uncertainty on R_b is ± 0.00041.

7.4 Simulation input parameters

The charm and light quark efficiencies are sensitive to the following simulation input parameters:

Charm quark fragmentation: The charm tagging efficiency ϵ^c increases with the scaled energy x_E of the weakly decaying charm hadron. The mean scaled energy $\langle x_E \rangle$ of charm hadrons produced in $c\bar{c}$ events at LEP has been measured by ALEPH, DELPHI and OPAL [18–20]. These measurements have been averaged by the LEP electroweak working group to give a value of $\langle x_E \rangle = 0.484 \pm 0.008$ for weakly decaying charm hadrons [21]. The effect of this uncertainty was assessed by reweighting events in the Monte Carlo changing $\langle x_E \rangle$ within this range. The fragmentation functions of Peterson [10], Collins and Spiller [22], Kartvelishvili [23] and the Lund group [24] were used as models to determine these event weights. The largest variation was found using the model of Collins and Spiller, and the resulting variation in R_b of ± 0.00028 was assigned as a systematic error. The charm fragmentation also affects the tagging efficiency via the number of tracks produced in the fragmentation process, but this effect was found to be much smaller than the direct energy dependence and was neglected.

Charm hadron production fractions: Because of the different charm hadron lifetimes and decay modes, the vertex tagging efficiency in $c\bar{c}$ events depends on the mixture of weakly decaying charm hadrons. The tagging efficiency for D^+ mesons is approximately three times that for D^0, whilst that for D_s^+ mesons is approximately 15% higher than D^0 and that for Λ_c^+ is only 15% of that for D^0. The fractions of D^+, D^0, D_s^+ and Λ_c^+ were varied according to the production fractions measured at LEP [19,25] as averaged by the LEP electroweak working group [21]. The contribution from Λ_c^+ was scaled by 1.15 ± 0.05 to account for other weakly decaying charm baryons. The errors were combined taking their correlations into account to give an error on R_b of ± 0.00031. The dependence of the tagging efficiency on the fraction of weakly decay-

ing charm hadrons produced via the decay of excited charm states (D^* and D^{**}) was found to be negligible. The systematic error on the lepton tagging efficiency in $c\bar{c}$ events is derived from the inclusive charm semileptonic branching fraction, which is in turn derived from the individual charm hadron semileptonic branching fractions (see below). This introduces an additional dependence on the charm hadron production fractions which is correlated with that from the vertex tag, taking the total error on R_b from this source to ± 0.00046.

Charm hadron lifetimes: The lifetimes of the weakly decaying charm hadrons were varied separately within the errors quoted by the Particle Data Group [26]. Their contributions to the error on R_b were added in quadrature to give an error on R_b of ± 0.00007.

Charm hadron charged decay multiplicity: The reconstructed secondary vertex track multiplicity N_s is required to be at least three, and is also used as an input to the vertex tag neural network. The tagging efficiency in $c\bar{c}$ events therefore depends strongly on the charged track multiplicity of charm hadron decays. The average charged track multiplicity of D^+, D^0 and D_s^+ decays (including the charged decay products of any produced K_s^0 mesons) has been measured by MARK III [27]. The average multiplicity in Monte Carlo events was varied within the range given by MARK III using several different reweighting schemes, keeping the inclusive branching ratios to K^0 and Λ constant for each charm hadron. For charm baryons, for which no measurements are available, a variation of ± 0.5 was taken. The variations for each charm hadron species were combined in quadrature to give an overall error on R_b of ± 0.00014.

Charm hadron neutral decay multiplicity: The charm tagging efficiency in the Monte Carlo is also observed to depend on the number of π^0 mesons produced in the decay, even at fixed charged decay multiplicity, as the number of π^0 mesons produced affects the amount of energy and transverse momentum available for the charged decay products. The average π^0 multiplicity in D^+, D^0 and D_s^+ decays has been measured by MARK III [27], but with large errors. However, for the D^+ (64 ± 5) %, and for the D^0 (76.2 ± 3.5) %, of the total decay width is to known exclusive final states, most of which have well measured branching fractions and low π^0 multiplicity [28].

For the D^+ and D^0, the error is assessed by varying the Monte Carlo π^0 multiplicity in the unmeasured decay final states so as to reproduce the total variation in π^0 multiplicity allowed by the MARK III measurements, and adding a small contribution due to π^0 multiplicity variation allowed by the measurement errors on the exclusive final state branching fractions. Since most of the decay modes with high tagging efficiency have well measured branching fractions, and the tagging efficiency for the unmeasured decay modes is lower than average, this procedure leads to total errors which are about half the size of those obtained by simply reweighting all decay final states to vary the π^0

multiplicity inclusively. The charged multiplicity and inclusive branching ratios to K^0 and Λ were held constant. The results of this procedure are systematic errors on R_{b} of ± 0.00016 for the D^+ and ± 0.00021 for the D^0. For the D_s^+, where only $(18 \pm 4)\%$ of the total decay width is measured, the inclusive reweighting technique is used, leading to an error on R_{b} of ± 0.00016. The error due to charm baryons is negligible, due to their low production fraction and tagging efficiency. These errors are combined in quadrature to give a total error on R_{b} of ± 0.00030.

Charm hadron to K^0 branching fraction: The inclusive branching ratios $B(D^+ \to K^0, \overline{K^0}+X)$ $B(D^0 \to K^0, \overline{K^0} + X)$, $B(D_s^+ \to K^0, \overline{K^0} + X)$ and $B(\Lambda_c^+ \to \Lambda + X)$ were varied independently within the errors given by the Particle Data Group [26], leaving the decay charged multiplicity distribution unaltered. The resulting variations in R_{b} were combined in quadrature to give a systematic error on R_{b} of ± 0.00015.

Charm semileptonic branching fraction: For semileptonic decays of charmed hadrons, an average branching fraction of $(9.3 \pm 0.5)\%$ was used. This value was obtained from two sources: the direct charm semileptonic branching fraction of $(9.5 \pm 0.9)\%$ measured at $\sqrt{s} = 10\,\mathrm{GeV}$ [29], and individual charm hadron branching fractions combined with the production fractions discussed above. The charm hadron semileptonic branching fractions were obtained from the branching fraction $D^0 \to e^+X$ of $(6.75 \pm 0.29)\%$ [26], together with the measured charm hadron lifetimes [26] and assumptions of lepton universality and equal semileptonic widths of all charm hadrons. This procedure gave a charm semileptonic branching fraction of $(9.1 \pm 0.6)\%$, which was averaged with the direct measurement. The direct measurement and $D^0 \to e^+$ branching ratio uncertainties give a systematic error of ± 0.00031 on R_{b} and an additional error of ± 0.00015 results from the uncertainty in the charm hadron production fractions.

Charm semileptonic decay modelling: The momentum spectra of the leptons in the rest frame of the decaying charmed hadrons were modified according to the refined free-quark model of Altarelli et al.[30]. The two parameters of the model, m_s and p_F, were chosen to be $0.001\,\mathrm{GeV}$ and $0.467\,\mathrm{GeV}$, respectively, as given by a fit to DELCO [31] and MARK III [32] data performed by the LEP electroweak working group. Two sets of alternative values of the parameters, $m_s = 0.001\,\mathrm{GeV}$, $p_F = 0.353\,\mathrm{GeV}$ and $m_s = 0.153\,\mathrm{GeV}$, $p_F = 0.467\,\mathrm{GeV}$, corresponding to the variation allowed by the fit, were used to estimate the systematic error on R_{b} of ± 0.00029.

Heavy quark production from gluon splitting:
The production of heavy quark pairs via the processes $g \to c\bar{c}$ and $g \to b\bar{b}$ increases the tagging efficiency in charm and light quark events. The rate of $g \to c\bar{c}$ per multihadronic event has been measured by OPAL to be $(2.38 \pm 0.48) \times 10^{-2}$ [33], consistent with perturbative QCD calculations [3]. The rate of $g \to b\bar{b}$ has

been measured by ALEPH and DELPHI [34] and has been averaged to give a value of $(2.56 \pm 0.67) \times 10^{-3}$ [21], also consistent with perturbative QCD calculations. The Monte Carlo rates were adjusted to these central values, and the uncertainties in the rates lead to errors on R_{b} of ± 0.00018 from $g \to c\bar{c}$ and ± 0.00027 from $g \to b\bar{b}$.

Inclusive K^0 and hyperon production: The total production rates of K^0, Λ and other weakly decaying hyperons in the Monte Carlo were adjusted to agree with the values measured by OPAL [35]. The rates were varied by $\pm 3.4\%$, $\pm 6.5\%$ and $\pm 11.5\%$ respectively, corresponding to the precision of the OPAL measurements combined with an additional uncertainty to take into account the extrapolation of the inclusive production rates to those for light quark events only. The results of these variations were combined in quadrature to give a systematic error on R_{b} of ± 0.00001. The dependence of the folded vertex tagging efficiencies on the number of tracks produced in light quark events was found to be negligible.

The finite number of charm and light quark Monte Carlo events contributes an additional error of ± 0.00010 on R_{b}.

8 Systematic errors: efficiency correlation

The tagging efficiency correlation C^{b} (as defined in Sect. 2) is determined from a sample of 7 million simulated $b\bar{b}$ events, with small corrections for the differing detector performance in each year. To evaluate the systematic error on this quantity, three classes of effect that can give rise to an efficiency correlation are considered: (1) kinematic correlations due to final state gluon radiation, (2) geometrical correlations due to detector non-uniformities, and (3) correlations coming from the determination of the primary vertex position. From Eq. (3) it can be seen that the fractional error on the correlation C^{b} contributes directly to the fractional error on R_{b}, so an accurate evaluation of C^{b} is essential.

In general, correlations arise when the tagging efficiency ϵ^{b} depends on a variable or variables x, and the values of x are correlated between the two hemispheres of the event. The resulting tagging efficiency correlation C^{b} can be evaluated as:

$$C^{\mathrm{b}} = \frac{\langle \epsilon^{\mathrm{b}}(x)\epsilon^{\mathrm{b}}(\overline{x}) \rangle}{\langle \epsilon^{\mathrm{b}}(x) \rangle \langle \epsilon^{\mathrm{b}}(\overline{x}) \rangle}$$

where x and $\overline{x}$ are the values of x in the two hemispheres of the event, and the average is taken over all $b\bar{b}$ events in the sample. Such calculations, with the efficiencies evaluated in small bins of x, are used frequently in the correlation studies presented here.

The total correlation estimates and errors are summarised in Table 6. The overall error on R_{b} resulting from uncertainties in the correlation values is ± 0.00066, corresponding to a relative uncertainty of 0.30%. The systematic errors are evaluated by studying each component

Table 6. Errors on the hemisphere efficiency correlation $C^{\mathrm{b}} - 1$ for the vertex and combined tags, together with the correlation values and associated total errors used for each year of the data. The latter are obtained using the geometrical correlation values given in Table 7

Uncertainty on $C^{\mathrm{b}} - 1$ (%)		Vertex	Combined
Kinematic	Same hemisphere events	0.08	0.06
	Momentum correlation	0.33	0.22
Geometrical	Systematic error	0.03	0.02
	Data statistics 1992	0.14	0.12
	Data statistics 1993	0.17	0.11
	Data statistics 1994	0.09	0.06
	Data statistics 1995	0.13	0.09
Primary vertex		0.02	0.02
Simulation	Detector resolution	0.01	0.02
	Beam spot size	0.04	0.06
	b quark fragmentation	0.09	0.08
	b hadron lifetime	0.04	0.03
	b decay multiplicity	0.01	0.01
Total systematic error		0.36	0.25
Monte Carlo statistics		0.20	0.17
Total Correlation $C^{\mathrm{b}} - 1$ (%)	1992	0.84 ± 0.42	1.01 ± 0.33
	1993	1.10 ± 0.44	1.13 ± 0.33
	1994	0.77 ± 0.41	0.92 ± 0.31
	1995	0.99 ± 0.42	0.95 ± 0.32

of the correlation separately. It is then checked that the total Monte Carlo correlation is reproduced by the sum of these components. The dependence of the Monte Carlo correlation on uncertainties in the detector simulation and physics modelling is also taken into account. This method differs from that used in [4], where only relatively small Monte Carlo samples were available, and the overall correlation was determined by adding the estimates of each separate correlation component. Interdependence between the correlation components was treated in [4] as an additional source of systematic error, but this is now accounted for by taking the correlation value directly from the Monte Carlo.

The evaluation of the kinematic correlation is described in detail in Sects. 8.1 and 8.2, and various comparisons between data and Monte Carlo are discussed in Sects. 8.3 and 8.4. The geometrical correlation, and the associated corrections to the Monte Carlo correlation value, are described in Sect. 8.5. Primary vertex effects are discussed in Sect. 8.6 and the detector simulation and physics modelling systematic errors in Sect. 8.7. The completeness test, that the total Monte Carlo correlation is consistent with the sum of the various components, is described in Sect. 8.8. Throughout this section, correlation values and uncertainties are given both for the vertex tag alone, and for the combined vertex and lepton tags.

8.1 Kinematic correlation – same-hemisphere events

If an energetic gluon is radiated in a $b\bar{b}$ event, it may cause both b hadrons to recoil into the same thrust hemisphere. The tagging efficiency for such hemispheres is lower than that for the average b hemisphere, since the b hadrons have much lower momentum, and the double tagging efficiency for these events is much lower than for normal $b\bar{b}$ events since one hemisphere contains no b hadrons. These events therefore introduce a small hemisphere efficiency correlation, which can be calculated in the Monte Carlo from the number of such events and their hemisphere and double tagging efficiencies. The Monte Carlo predicts that 1.21 % of $b\bar{b}$ events passing the event selection have both b hadrons in the same hemisphere. However, such events constitute only 0.59 % of the tagged hemispheres and 0.003 % of the double tagged events for the vertex tag, and only 0.62 % and 0.014 % for the combined tag. They contribute (0.02 ± 0.02) % to the tagging efficiency correlation for the vertex tag and (-0.03 ± 0.02) % for the combined tag, where the errors are due to Monte Carlo statistics.

The number of same hemisphere events was compared in data and Monte Carlo by looking for events with two vertex tags in the same hemisphere, each passing a very loose neural network output cut of $B > 0.5$. In the Monte Carlo, 36 % of these double tagged hemispheres come from genuine same-hemisphere events, 40 % from normal $b\bar{b}$ events with a mis-reconstructed vertex, and 23 % from charm and light quark events. The different contributions
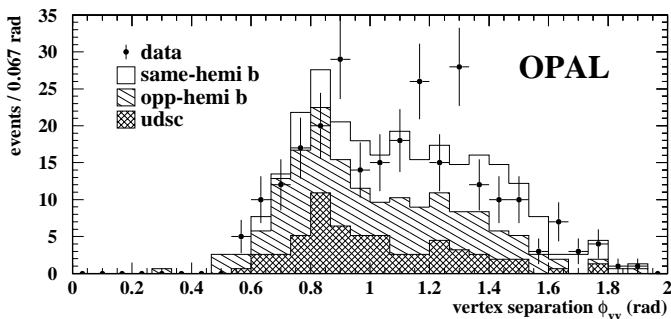
Fig. 8. Distribution of the separation angle ϕ_{vv} between two vertices loosely tagged in the same hemisphere for genuine same-hemisphere $b\bar{b}$ events, normal opposite hemisphere $b\bar{b}$ events, charm and light quark events and data

were statistically separated using the three-dimensional angle ϕ_{vv} between the momentum vectors of the two vertices; the same-hemisphere $b\bar{b}$ events have a relatively broad ϕ_{vv} distribution and the remaining contributions are more concentrated at low values of ϕ_{vv}. The distribution of ϕ_{vv} for the double tagged hemispheres in data and Monte Carlo is shown in Fig. 8. The ϕ_{vv} distribution in the data was fitted to the sum of the Monte Carlo distributions, allowing the rate of the Monte Carlo same hemisphere $b\bar{b}$ events to vary. The rate of genuine same hemisphere events was found to be consistent between data and Monte Carlo with a statistical uncertainty of $\pm 40\%$. The systematic error due to uncertainties in the momentum distribution of the b hadrons was evaluated by comparing the predictions of JETSET 7.4 and HER-WIG 5.9 [36]. This gives a 7% relative uncertainty on the vertex tagging efficiency for same hemisphere events, and a 5% uncertainty for the combined tag. The resulting total uncertainty on the size of the same hemisphere event correlation is $\pm 0.08\%$ for the vertex tag and $\pm 0.06\%$ for the combined tag. The tagging efficiencies are also sensitive to the modelling of b hadron decay in the Monte Carlo, but this is addressed in Sect. 8.7.

8.2 Kinematic correlation – momentum and fragmentation

After removing the same-hemisphere events in the Monte Carlo, each hemisphere of a $b\bar{b}$ event contains one b hadron. Kinematic variables, such as the momenta of the two b hadrons p_B and $p_{\bar{B}}$, are correlated between the two hemispheres due to final state gluon radiation. Since the b-tagging efficiency depends on these kinematic variables, such correlations can produce a tagging efficiency correlation.

The b-tagging efficiency depends strongly on the b hadron momentum in the same hemisphere, since high-momentum b hadrons are likely to travel further before decaying, and decay producing higher momentum tracks which are measured with better resolution. Both of these effects produce a more easily resolvable secondary vertex. The efficiency is shown as a function of $x_B = p_B/E_{beam}$
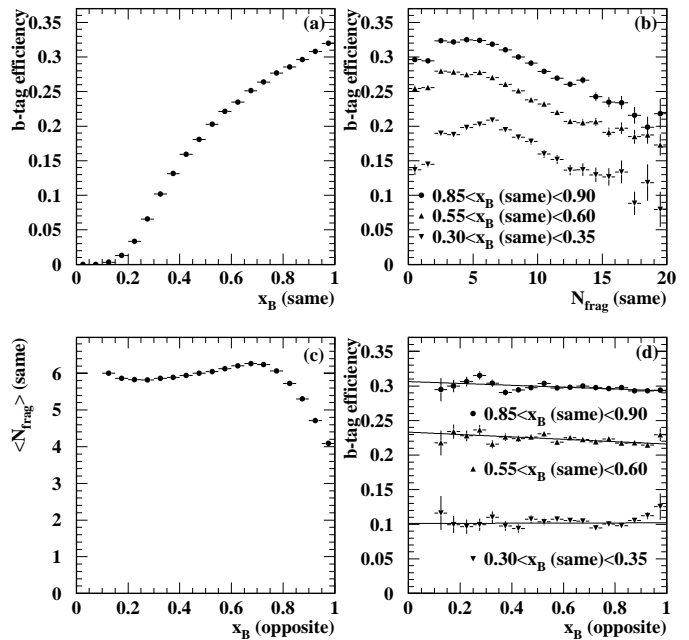

Fig. 9a–d. Origins of kinematic correlations in Monte Carlo $b\bar{b}$ events: **a** Dependence of b-tagging efficiency ϵ^b on the scaled b hadron momentum $x_B = p_B/E_{beam}$ in the same hemisphere; **b** dependence of ϵ^b on the number of fragmentation tracks N_{frag} in the same hemisphere, at various values of x_B in the same hemisphere; **c** variation in the mean number of fragmentation tracks $\langle N_{frag}\rangle$ with x_B in the opposite hemisphere; **d** dependence of ϵ^b on x_B in the opposite hemisphere, at various values of x_B in the same hemisphere

for the combined vertex and lepton tag in Fig. 9a. However, the b-tagging efficiency also depends on properties of the fragmentation tracks in the same hemisphere, for example their number, momentum and angular distribution, which influence the reconstruction of the primary and secondary vertices. The dependence of the b-tagging efficiency on the number of fragmentation tracks N_{frag} is shown in Fig. 9b. Although N_{frag} is negatively correlated with p_B there is a dependence even at constant p_B. As the number of fragmentation tracks in a hemisphere increases, the vertex tagging algorithm becomes increasingly likely to reconstruct the primary rather than the secondary vertex, and is therefore less likely to give a b-tag.

Final state gluon radiation into one hemisphere decreases the momentum of the b hadron in that hemisphere, and increases the number of fragmentation tracks. It will also increase the hemisphere mass $m_h = \sqrt{E_h^2 - p_h^2}$ where E_h and p_h are the total energy and momentum in the hemisphere. Since the total momenta of the two hemispheres must balance, this will also reduce the total momentum, and hence the momentum available to the b hadron, in the opposite hemisphere of the event. Therefore the momentum p_B of the b hadron in one hemisphere is correlated both with the momentum $p_{\bar{B}}$ of the b hadron and the number of fragmentation tracks $N_{\overline{frag}}$ in the opposite hemisphere. This can be seen in Fig. 9c, where the Monte Carlo dependence of N_{frag} in one hemisphere on

$p_{\bar{\text{B}}}$ in the other hemisphere is shown. At moderate values of $p_{\bar{\text{B}}}$, $\langle N_{\text{frag}} \rangle$ increases with increasing $p_{\bar{\text{B}}}$ and it then decreases again at very high values of $p_{\bar{\text{B}}}$.

As a result of these correlations, the b-tagging efficiency is found to depend not only on the same hemisphere b hadron momentum p_{B}, but also weakly on the opposite hemisphere b hadron momentum $p_{\bar{\text{B}}}$, as shown in Fig. 9d. This effect was also seen with the much simpler vertex tagging algorithm used in [4]. The resulting kinematic correlation can be calculated by parameterising the b-tagging efficiency as a function of both p_{B} and $p_{\bar{\text{B}}}$, and is given by:

$$C_{p,\bar{p}}^{\text{b}} = \frac{\langle \epsilon^{\text{b}}(p_{\text{B}}, p_{\bar{\text{B}}}) \epsilon^{\text{b}}(p_{\bar{\text{B}}}, p_{\text{B}}) \rangle}{\langle \epsilon^{\text{b}}(p_{\text{B}}, p_{\bar{\text{B}}}) \rangle \langle \epsilon^{\text{b}}(p_{\bar{\text{B}}}, p_{\text{B}}) \rangle}, \qquad (4)$$

where $\epsilon^{\text{b}}(p_1, p_2)$ gives the b-tagging efficiency for a hemisphere containing a b hadron of momentum p_1, the other hemisphere of the event containing a b hadron of momentum p_2, and the averages are taken over all $b\bar{b}$ events in the sample. The Monte Carlo predicts that the kinematic efficiency correlation is $C_{p,\bar{p}}^{\text{b}} - 1 = (0.04 \pm 0.05)\,\%$ for the vertex tag and $C_{p,\bar{p}}^{\text{b}} - 1 = (0.06 \pm 0.03)\,\%$ for the combined tag.

The size of the underlying momentum correlation between p_{B} and $p_{\bar{\text{B}}}$ is given by:

$$C p_{\text{B}} = \frac{\langle p_{\text{B}}\, p_{\bar{\text{B}}} \rangle}{\langle p_{\text{B}} \rangle \langle p_{\bar{\text{B}}} \rangle},$$

and the size of the resulting efficiency correlation, if the b-tagging efficiency depended only on the same hemisphere b hadron momentum, would be:

$$C_p^{\text{b}} = \frac{\langle \epsilon^{\text{b}}(p_{\text{B}})\, \epsilon^{\text{b}}(p_{\bar{\text{B}}}) \rangle}{\langle \epsilon^{\text{b}}(p_{\text{B}}) \rangle \langle \epsilon^{\text{b}}(p_{\bar{\text{B}}}) \rangle}, \qquad (5)$$

The Monte Carlo predicts a b hadron momentum correlation of $C p_{\text{B}} - 1 = (0.80 \pm 0.01)\,\%$, in agreement with perturbative QCD calculations [37]. This would result in a tagging efficiency correlation of $C_p^{\text{b}} - 1 = (0.87 \pm 0.03)\,\%$ for the vertex tag and $C_p^{\text{b}} - 1 = (0.55 \pm 0.03)\,\%$ for the combined vertex and lepton tag. The additional dependence of the tagging efficiency on $p_{\bar{\text{B}}}$ via the fragmentation tracks reduces this correlation, to give an overall effect which is approximately zero. However, both the size of the momentum correlation $C p_{\text{B}}$ and the separate correlation between N_{frag} and $p_{\bar{\text{B}}}$ are tested when calculating the systematic error. This is discussed in Sect. 8.3 below.

The momentum correlation has been treated above in terms of p_{B} and N_{frag}, quantities on which the tagging efficiency depends strongly, but whose hemisphere correlations are weak and difficult to measure. A different and complementary approach is provided by considering the total energy E_{h} and momentum p_{h} in each hemisphere, which are completely correlated by overall energy and momentum conservation in the event, and are affected by final state gluon radiation. These variables should give a good description of the kinematic correlation resulting purely from energy and momentum conservation. The variables E_{h} and p_{h} are relatively easy to measure in the data, and the two hemispheres are related by $E_{\text{h}} + E_{\bar{\text{h}}} = 2 E_{\text{beam}}$ and $p_{\text{h}} = p_{\bar{\text{h}}}$. However, the dependence of the tagging efficiency on these quantities is weaker than that on p_{B} and N_{frag}.

In this approach, the kinematic correlation resulting from energy and momentum conservation may be calculated by parameterising the tagging efficiencies in terms of E_{h} and p_{h}:

$$C_{E,p}^{\text{b}} = \frac{\langle \epsilon^{\text{b}}(E_{\text{h}}, p_{\text{h}}) \epsilon^{\text{b}}(E_{\bar{\text{h}}}, p_{\bar{\text{h}}}) \rangle}{\langle \epsilon^{\text{b}}(E_{\text{h}}, p_{\text{h}}) \rangle \langle \epsilon^{\text{b}}(E_{\bar{\text{h}}}, p_{\bar{\text{h}}}) \rangle}, \qquad (6)$$

The Monte Carlo predicts that $C_{E,p}^{\text{b}} - 1 = (-0.27 \pm 0.04)\,\%$ for the vertex tag and $(-0.14 \pm 0.04)\,\%$ for the combined tag. If the efficiency is parameterised in terms of the hemisphere momentum p_{h} alone, the correlation is $(1.34 \pm 0.03)\,\%$ for the vertex tag and $(0.85 \pm 0.03)\,\%$ for the combined tag, somewhat larger than the values obtained for C_p^{b} using the b hadron momentum p_{B} alone.

The kinematic correlation $C_{E,p}^{\text{b}} - 1$ is significantly more negative than $C_{p,\bar{p}}^{\text{b}} - 1$. To study whether significant additional correlation, other than that caused by energy and momentum conservation, is present in the Monte Carlo, the correlation $C p_{\text{B}}$ between p_{B} and $p_{\bar{\text{B}}}$ was evaluated in bins of E_{h} and p_{h}. For the majority of the events, no significant additional correlation was observed, but for events with low values of p_{h}, *i.e.* those with broad high mass jets in both hemispheres, a significant positive correlation between p_{B} and $p_{\bar{\text{B}}}$ was observed. This gives an extra contribution of about $+0.15\,\%$ to the tagging efficiency correlation, bringing the overall kinematic correlation closer to that calculated from p_{B} and $p_{\bar{\text{B}}}$ above.

Both of the approaches described above were used to study correlations in the data. The correlations between p_{B} and $p_{\bar{\text{B}}}$, and between N_{frag} and $p_{\bar{\text{B}}}$, were checked using estimators of these quantities in a sample of loose double tagged events (see Sect. 8.3). The distributions of p_{h} and E_{h}, and the dependence of the tagging rates on them were studied. Monte Carlo events were reweighted to make the various distributions the same as those in the data, and the resulting changes in the correlation evaluated (see Sect. 8.4). Since all of the tests are somewhat indirect, and all the possible sources of kinematic correlations have not been completely understood, the largest systematic error resulting from any of the tests is used as the overall systematic error on the kinematic correlation. As can be seen from Table 6, the resulting systematic error is similar in size to the uncertainty in the correlation from Monte Carlo statistics.

8.3 Kinematic correlation tests
– b momentum and fragmentation

In order to study correlations in the data, a loose double tag was used to select a sample of almost pure $b\bar{b}$ events. Events were selected if each hemisphere contained a secondary vertex passing the neural network pre-selection described in Sect. 4.2, *i.e.* at least three tracks with a decay
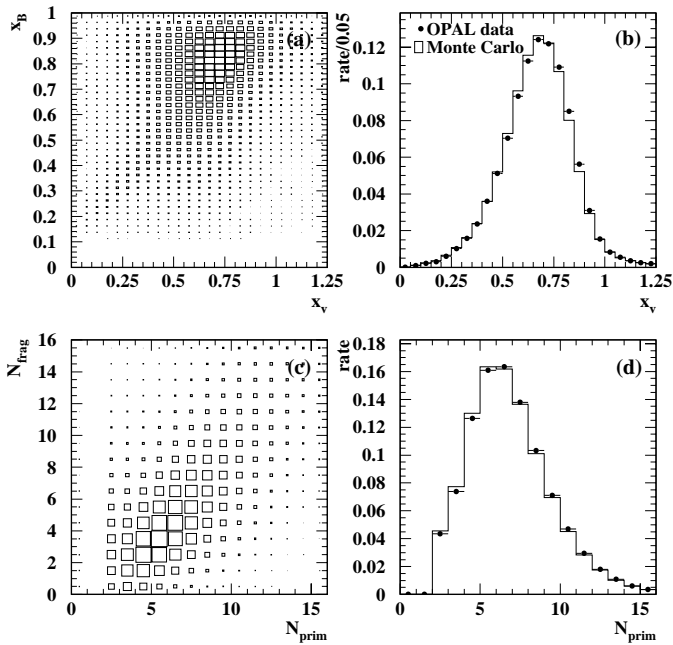
Fig. 10a–d. Estimators of of the scaled b hadron momentum x_B and number of fragmentation tracks N_{frag}: **a** correlation of estimated x_B (x_v) with true x_B (b) distributions of x_v in data (points) and Monte Carlo (histogram), **c** correlation of estimated N_{frag} (N_{prim}) and true N_{frag}, **d** distributions of N_{prim} in data and Monte Carlo

length significance of at least $|L/\sigma| > 3$, or a lepton passing the selection described in Sect. 5. This selection has an efficiency for b$\bar{\mathrm{b}}$ events of about 31 % and a b purity of about 95 %.

Reconstructed secondary vertices were then used to form estimates p_v of the corresponding b hadron momentum. The component of the b hadron's momentum associated with charged particles was estimated by summing the momenta of all charged particles in the jet, each weighted by X—the weight for the track to have come from the b hadron decay described in Sect. 4.3. The neutral momentum component was estimated using the energy of all the electromagnetic calorimeter clusters in the jet, each weighted as a function of the angle between the cluster and the jet axis. If any charged tracks were associated to the cluster, their energies were first subtracted from the cluster energy, and the cluster was only used if the remaining energy was greater than zero. If the hemisphere was tagged only by a lepton, the lepton momentum was used as the p_v estimator. The lepton momentum was scaled to give the same mean value of p_v as that from reconstructed vertices. The correlation of $x_v = p_v/E_{\mathrm{beam}}$ with $x_B = p_B/E_{\mathrm{beam}}$ is shown in Fig. 10a, and the distribution of x_v in data and Monte Carlo loose double-tagged events is shown in Fig. 10b. The correlation coefficient $\rho = (\langle p_B p_v \rangle - \langle p_B \rangle \langle p_v \rangle)/(\sigma_{p_B} \sigma_{p_v})$ of the two quantities is 0.34, where σ_{p_B} and σ_{p_v} are the standard deviations of p_B and p_v respectively.

The number of tracks assigned to the hemisphere primary vertex N_{prim} was used as an estimator of the number

of fragmentation tracks N_{frag} in the hemisphere. The correlation of N_{prim} with N_{frag} is shown in Fig. 10c, and the distribution of N_{prim} in data and Monte Carlo in Fig. 10d. The correlation coefficient of N_{prim} and N_{frag} is 0.68.

The correlation of the estimated b hadron momentum in one hemisphere, p_v, with the estimated b hadron momentum in the other hemisphere, $p_{\bar{v}}$ was measured to be $Cp_v - 1 = (0.670 \pm 0.023)$ % in the loose double tagged data sample, and $Cp_v - 1 = (0.664 \pm 0.015)$ % in the corresponding Monte Carlo sample. The effects of including the same-hemisphere events and the non-b$\bar{\mathrm{b}}$ background were checked in the Monte Carlo and found to be negligible. The Monte Carlo is therefore seen to reproduce the strength of the correlation between p_v and $p_{\bar{v}}$ seen in the data. Since p_v is only an estimate of p_B the Monte Carlo was reweighted to change the true correlation between p_B and $p_{\bar{B}}$ and the resulting changes in C_{p_v} and the efficiency correlation C_p^b studied. The statistical error on the difference between C_{p_v} in data and Monte Carlo corresponds to an uncertainty of ± 0.27 % in C_p^b for the vertex tag and ± 0.19 % for the combined tag.

The size of the correlation between N_{frag} and the opposite hemisphere b hadron momentum was also studied using the estimators described above. The average values of N_{prim} as a function of the estimated opposite hemisphere b momentum are shown in Fig. 11a for the Monte Carlo and Fig. 11b for the data loose double tagged samples. A complicated correlation is seen in both data and Monte Carlo, with the value of $\langle N_{\mathrm{prim}} \rangle$ increasing in the region $0.2 < x_v < 0.5$ and then decreasing again in the region $0.5 < x_v < 0.8$. Qualitatively similar behaviour is also seen in the variation of $\langle N_{\mathrm{frag}} \rangle$ with x_B shown in Fig. 9c.

Two methods were used to compare the strength of the $N_{\mathrm{frag}}, p_{\bar{B}}$ correlations seen in data and Monte Carlo. In the first method, the distributions were fitted to a parabola in the region $0.3 < x_v < 0.8$ (where the bulk of the events lie), and the curvatures compared. The ratio between data and Monte Carlo curvatures was found to be 0.85 ± 0.10. In the second method, the root mean square deviation of $\langle N_{\mathrm{prim}} \rangle (x_v)$ from $\langle \langle N_{\mathrm{prim}} \rangle \rangle$ was calculated, weighted according to the distribution of x_v. Here, $\langle N_{\mathrm{prim}} \rangle (x_v)$ is the average value of N_{prim} at a particular value of x_v, and $\langle \langle N_{\mathrm{prim}} \rangle \rangle$ is the average of N_{prim} calculated over all events. This method also takes into account the events outside the region $0.3 < x_v < 0.8$, and gives a ratio between data and Monte Carlo of 0.91. The Monte Carlo was then reweighted to change the correlation between N_{frag} and $p_{\bar{B}}$, and the variation of the difference $C_{p,\bar{p}}^b - C_p^b$ studied. The full variation between the unweighted Monte Carlo sample and the sample reweighted to reduce the correlation between N_{prim} and $p_{\bar{v}}$ by 25 % was used to estimate the systematic error on $C_{p,\bar{p}}^b - C_p^b$, giving uncertainties of ± 0.20 % and ± 0.12 % for the vertex and combined tags respectively.

The uncertainties on the separate components of the kinematic correlation C_p^b and $C_{p,\bar{p}}^b - C_p^b$ were then added in quadrature to give total uncertainties on the kinematic correlation of 0.33 % and 0.22 % for the vertex and com-
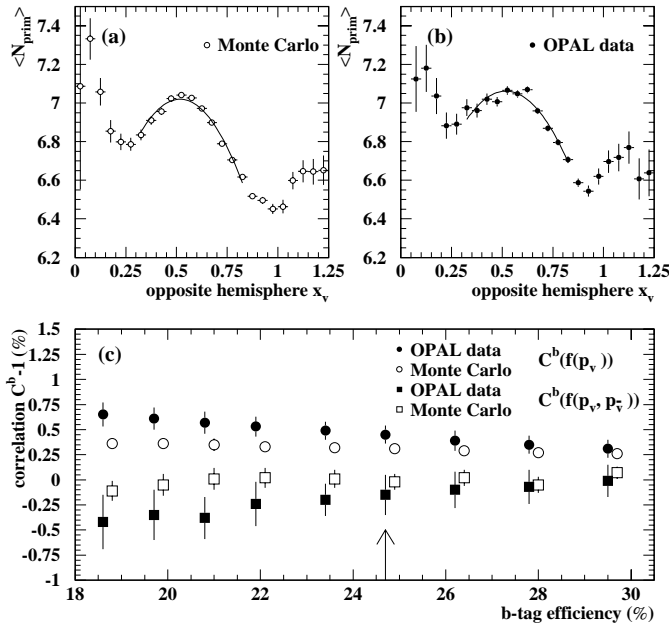
Fig. 11a–d. Estimated $\langle N_\mathrm{frag} \rangle$ as a function of the estimated opposite hemisphere scaled momentum x_B, in loose double tagged Monte Carlo **a** and data **b** samples. The fits used to estimate the size of the correlation are shown. **c** Hemisphere tagging efficiency correlations $C^\mathrm{b} - 1$ calculated using the estimated b hadron momentum p_v, as a function of p_v only in the tagging hemisphere (circles), and in both the tagging and opposite hemispheres (squares). The data is shown by the filled symbols and the Monte Carlo by the open symbols. The errors are highly correlated between the points of different b-tagging efficiency, and the analysis cut is shown by the arrow. The individual points are slightly displaced along the x-axis for clarity

bined tags respectively. These uncertainties are the largest from any of the correlation tests, and set the size of the overall systematic error. The uncertainty for the vertex tag alone is somewhat larger for two reasons: the lepton tag has a weaker dependence on the b hadron momentum and no dependence on the number of fragmentation tracks; and the comparisons between data and Monte Carlo are dominated by the statistical precision of the tests, which are improved by adding the extra lepton tagged hemispheres.

As an alternative approach, the distributions of p_v and N_prim were studied in data and Monte Carlo, and the influence of discrepancies in these distributions on the kinematic correlation investigated. In this approach, the decomposition of the kinematic correlation into the C^b_p and $C^\mathrm{b}_{p,\bar{p}} - C^\mathrm{b}_p$ components was not used. Event weights were calculated for the Monte Carlo to make the distributions of p_v and N_prim match those in the data, and the resulting kinematic correlation calculated and compared with the value derived using:

$$C^\mathrm{b}_{p_\mathrm{v},p_\mathrm{v}} = \frac{\langle \epsilon^\mathrm{b}(p_\mathrm{v},p_{\bar{\mathrm{v}}})\epsilon^\mathrm{b}(p_{\bar{\mathrm{v}}},p_\mathrm{v})\rangle}{\langle \epsilon^\mathrm{b}(p_\mathrm{v},p_{\bar{\mathrm{v}}})\rangle\langle \epsilon^\mathrm{b}(p_{\bar{\mathrm{v}}},p_\mathrm{v})\rangle}$$

i.e. the same as (4), but with p_B and $p_{\bar{\mathrm{B}}}$ replaced by the estimators p_v and $p_{\bar{\mathrm{v}}}$ and the averages taken over the sample

of loose double tagged events. Event weights and efficiencies were calculated as a function of p_v and $p_{\bar{\mathrm{v}}}$, p_v and N_prim, and N_prim and $N_{\overline{\mathrm{prim}}}$, and the largest changes seen in $C^\mathrm{b}_{p_\mathrm{v},p_\mathrm{v}}$ were 0.11 % and 0.07 % for the vertex and combined tags respectively, well within the systematic errors assigned for the kinematic correlation.

Finally, the hemisphere tagging efficiency relative to the loose double tag pre-selection was calculated directly in the data and Monte Carlo, from the fraction of events tagged as a function of p_v, or of p_v and $p_{\bar{\mathrm{v}}}$. The two dimensional distribution of p_v and $p_{\bar{\mathrm{v}}}$ can then be used to derive an effective tagging efficiency correlation. The results of this procedure are shown in Fig. 11c. The circles show the correlation calculated using the momentum dependence of the tagging efficiency in the tag hemisphere only:

$$C^\mathrm{b}(f(p_\mathrm{v})) = \frac{\langle f(p_\mathrm{v})f(p_{\bar{\mathrm{v}}})\rangle}{\langle f(p_\mathrm{v})\rangle\langle f(p_{\bar{\mathrm{v}}})\rangle},$$

where $f(p_\mathrm{v})$ is the fraction of hemispheres of estimated b hadron momentum p_v that are tagged. The squares show the correlation calculated using the momentum dependence of the tagging efficiency in both hemispheres:

$$C^\mathrm{b}(f(p_\mathrm{v},p_{\bar{\mathrm{v}}})) = \frac{\langle f(p_\mathrm{v},p_{\bar{\mathrm{v}}})f(p_{\bar{\mathrm{v}}},p_\mathrm{v})\rangle}{\langle f(p_\mathrm{v},p_{\bar{\mathrm{v}}})\rangle\langle f(p_{\bar{\mathrm{v}}},p_\mathrm{v})\rangle}.$$

In both cases, the correlations calculated from data and Monte Carlo are similar, and the increasing size of the correlation as the b-tagging efficiency is reduced is well modelled. The correlation using the tagging hemisphere momentum dependence alone is similar to that obtained in the Monte Carlo using the true b hadron momentum. The correlation due to the momentum dependence in both hemispheres is much closer to zero, again as in the Monte Carlo using the true b hadron momentum, though the statistical precision of this test is rather low.

8.4 Kinematic correlation tests – hemisphere energy and momentum

To study the correlations expressed in terms of hemisphere energy and momentum, estimates were formed of the total energy and momentum in each hemisphere using both tracking and calorimeter information, and applying an algorithm to correct for double counting of charged particles [38]. These reconstructed energy and momentum distributions have widths of about 7 GeV and are dominated by the experimental resolution. Since the hemisphere correlations of these quantities are known, the resolution of the estimators can be improved using information from both hemispheres and the beam energy constraint. This is done by calculating the two hemisphere masses m_h and $m_{\bar{\mathrm{h}}}$, using the beam energy to scale the total observed energy:

$$m_\mathrm{h} = \frac{2E_\mathrm{beam}}{E_\mathrm{h} + E_{\bar{\mathrm{h}}}}\sqrt{E_\mathrm{h}^2 - p_\mathrm{h}^2}$$

and then recalculating the hemisphere energies and momenta, using the two hemisphere masses, the known beam
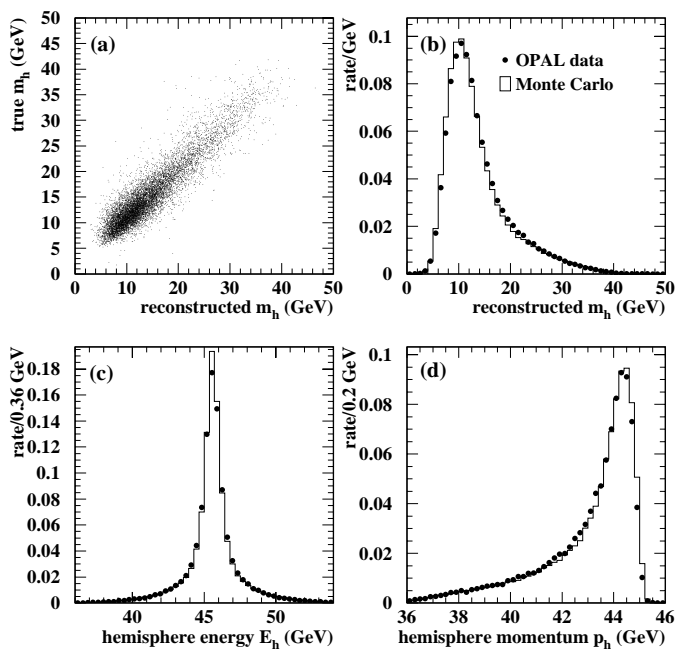
Fig. 12. a Correlation of reconstructed and true hemisphere masses m_{h}; **b–d** Distributions of reconstructed hemisphere mass, energy and momentum in loose double tagged events in data (points) and Monte Carlo (histogram)

Fig. 13a,b. Fractions of tagged hemispheres in loose double tagged events as functions of **a** hemisphere energy E_{h} and **b** hemisphere momentum p_{h}. The data are shown by the points and Monte Carlo by the histograms

8.5 Geometrical correlation

The two b hadrons in a $b\bar{b}$ event tend to be produced back-to-back, so their decay products are likely to hit geometrically opposite parts of the detector. This introduces an efficiency correlation if the tagging efficiency is not directionally uniform. The vertex tag efficiency depends on the polar angle θ of the b hadron because multiple scattering degrades the tracking resolution more as $\cos\theta$ increases. For some of the data, the tagging efficiency also depends on ϕ, due to inefficient regions of the silicon detector. The lepton tag efficiency depends on both θ and ϕ, due to localised regions of inefficiency caused by effects such as incomplete muon chamber coverage.

The size of the correlation from this effect can be estimated from the data, by measuring the hemisphere tagging probability as a function of the thrust axis polar angle θ_T and azimuthal angle ϕ_T:

$$C_{\mathrm{geom}}^{\mathrm{b}} = \tag{7}$$

$$\frac{4\langle f^+(\theta_T,\phi_T)f^-(\theta_T,\phi_T)\rangle}{\langle f^+(\theta_T,\phi_T)+f^-(\theta_T,\phi_T)\rangle\langle f^+(\theta_T,\phi_T)+f^-(\theta_T,\phi_T)\rangle}$$

where f^+ (f^-) is the fraction of hemispheres in the $+z$ $(-z)$ direction that are tagged, and the averages are performed over all values of $\cos\theta_T$ and ϕ_T. The values of f^+ and f^- are calculated in small bins of $\cos\theta_T$ and ϕ_T. As the tagged samples are very pure in $b\bar{b}$ events, contributions from charm and light flavour events to the correlations calculated from the tagged data are negligible.

The resulting geometrical correlations for the vertex, lepton and combined tags are given for each year of the data in Table 7. The values for the different years are consistent, and in agreement with those derived from Monte Carlo simulation of the detector configuration in each year.

In order to calculate the overall correlation coefficient appropriate for each year of the data, the geometrical correlation in the Monte Carlo sample was calculated using (7). These values are also given in Table 7. A correction:

$$\Delta C^{\mathrm{b}} = C_{\mathrm{geom}}^{\mathrm{b,data}} - C_{\mathrm{geom}}^{\mathrm{b,MC}} \tag{8}$$

energy and two-body decay kinematics. The correlation of the reconstructed hemisphere mass with the true mass in Monte Carlo $b\bar{b}$ events is shown in Fig. 12a, and the reconstructed mass distributions for the loose double tagged data and Monte Carlo samples in Fig. 12b.

The resulting distributions of hemisphere energies and momenta are shown in Fig. 12c and d. The resolutions of the estimators of hemisphere energy and momentum are $0.82\,\mathrm{GeV}$ and $0.68\,\mathrm{GeV}$ respectively, where the true quantities include unmeasured particles such as neutrinos. Some discrepancies are seen between the data and Monte Carlo distributions, which are addressed in the systematic error evaluation below.

The systematic error on $C_{E,p}^{\mathrm{b}}$ is evaluated in two steps. First, the two-dimensional distribution of hemisphere energies E_{h} and momenta p_{h} is reweighted in the loose double tagged Monte Carlo to match that of the data. This gives a shift in $C_{E,p}^{\mathrm{b}}$ of $(+0.08\pm0.01)\,\%$ for the vertex tag and $(+0.04\pm0.01)\,\%$ for the combined tag, where the errors are due to data and Monte Carlo statistics. Secondly, the modelling of the tag efficiency as a function of E_{h} and p_{h} is checked, by studying the fraction of tagged hemispheres as a function of E_{h} and p_{h} in data and Monte Carlo, as shown in Fig. 13. Reweighting the Monte Carlo to make the two dimensional distribution of the tag fraction as a function of E_{h} and p_{h} agree results in a change in $C_{E,p}^{\mathrm{b}}$ of $(+0.03\pm0.15)\,\%$ for the vertex tag and $(+0.03\pm0.13)\,\%$ for the combined tag, where the errors are statistical. These changes are all small, and well within the overall systematic errors assigned for the kinematic correlation.
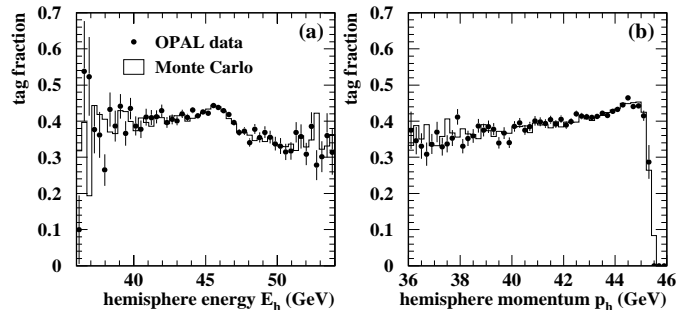
Table 7. Geometrical hemisphere efficiency correlations $C_{geom}^b - 1$ and their statistical errors, evaluated from each year of the data and from the Monte Carlo $b\overline{b}$ sample

Tag		1992	1993	1994	1995	Monte Carlo
Vertex	$C_{geom}^b - 1$ (%)	0.89 ± 0.14	1.15 ± 0.17	0.82 ± 0.09	1.04 ± 0.13	0.88 ± 0.02
Lepton	$C_{geom}^b - 1$ (%)	1.02 ± 0.36	0.54 ± 0.30	0.33 ± 0.18	0.12 ± 0.29	0.31 ± 0.03
Combined	$C_{geom}^b - 1$ (%)	0.79 ± 0.12	0.91 ± 0.11	0.70 ± 0.06	0.73 ± 0.09	0.71 ± 0.02

was then applied to the overall Monte Carlo correlation to give the final correlation value for each year of the data shown in Table 6.

The geometrical correlation is calculated using the thrust axis as an estimator of the b hadron direction, assuming the two b hadrons to be back to back. Final state gluon radiation can push the two b hadrons away from the thrust axis direction, and towards regions of the detector with different b tagging efficiency. The size of the true geometrical correlation is therefore given not by (7) but by:

$$C_{geom}^b = \frac{\langle \epsilon^b(\cos\theta_B, \phi_B) \epsilon^b(\cos\theta_{\bar{B}}, \phi_{\bar{B}}) \rangle}{\langle \epsilon^b(\cos\theta_B, \phi_B) \rangle \langle \epsilon^b(\cos\theta_{\bar{B}}, \phi_{\bar{B}}) \rangle}, \qquad (9)$$

where $\cos\theta_B$, ϕ_B and $\cos\theta_{\bar{B}}$, $\phi_{\bar{B}}$ give the directions of the two b hadrons, approximated by the thrust axis direction in (7). The error due to this approximation was estimated by calculating ΔC^b using (8), but with $C_{geom}^{b,data}$ replaced by $C_{geom}^{b,MC}$ calculated from an independent Monte Carlo sample with a geometrical correlation twice as strong as that seen in the data samples. The value of ΔC^b calculated using the thrust axis direction was then compared with that calculated using the true b-hadron directions, evaluating the two $C_{geom}^{b,MC}$ values using (9). The difference was 0.03 % for the vertex tag alone and 0.02 % for the combined tag, which was taken as the systematic error on the geometrical correlation correction.

8.6 Primary vertex correlation

In the previous analysis [4], the primary vertex position was determined using all tracks in the event, and then used in the tagging of each hemisphere. This led to a small but significant negative efficiency correlation. In this analysis, the primary vertex correlation has been largely eliminated by determining the primary vertex separately for each hemisphere (see Sect. 4.1). However, the beam spot constraint is still shared between the hemispheres, which may lead to a small residual correlation.

This was investigated in the Monte Carlo by generating separate independent beam spot constraints for each hemisphere, according to a Gaussian distribution of the same width as the usual beam spot constraint, centred about the true event primary vertex position. This procedure retains the constraint from the beam spot but removes any correlation due to the shared position information. The Monte Carlo tagging efficiency correlation using this modified constraint was found to be different by

only 0.02 % from that with the normal constraint, showing there is no significant primary vertex correlation from the shared beamspot. The full size of this shift is taken as an additional systematic error on the overall correlation value.

8.7 Correlation simulation systematics

The estimate of the overall size of the efficiency correlation from the Monte Carlo relies on the detector simulation and the modelling of the production and decay of b hadrons. The following uncertainties were considered to estimate the systematic error from these sources. The effect of each variation on the correlation values is given in Table 6.

Detector resolution: The detector resolution was varied using the method discussed in Sect. 7.1, varying the r-ϕ resolution parameter in the range 0.9–1.1. Since the effect seen is very small, additional studies varying the r-z tracking resolution, tracking efficiency, silicon alignment and silicon hit matching efficiency were not carried out.

Beam spot size: The size of the LEP beam spot varied between each year of the data due to the differing operating conditions of the accelerator. The beam spot size was measured in each year using $Z^0 \rightarrow \mu^+\mu^-$ events, and was typically $140\,\mu m$ in x, $10\,\mu m$ in y, and $7\,mm$ in z. In x and z, the beam spot size also decreases gradually during the course of each fill, due to the operation of the LEP wiggler magnets. Residual uncertainties in the beam spot size are estimated to be $\pm 10\,\mu m$ in x, $\pm 5\,\mu m$ in y and $\pm 1\,mm$ in z. The effective beam spot constraint in Monte Carlo events was varied by these amounts to assess the resulting uncertainty in the correlation coefficients.

b quark fragmentation: The b quark fragmentation was varied in the Monte Carlo by applying a weight to each simulated event using the fragmentation functions discussed in Sect. 7.4, so as to vary the average scaled energy $\langle x_E \rangle$ of the weakly decaying b hadrons by ± 0.008. This variation represents the accuracy of $\langle x_E \rangle$ measured by LEP experiments [39,18].

b hadron lifetime: The lifetimes of the b hadrons were varied simultaneously by $\pm 0.05\,ps$ using a weighting method. The size of the variation was chosen to be larger than the accuracy of the world average b-lifetime [26] to allow for the uncertainties due to different efficiencies for different b hadron species.

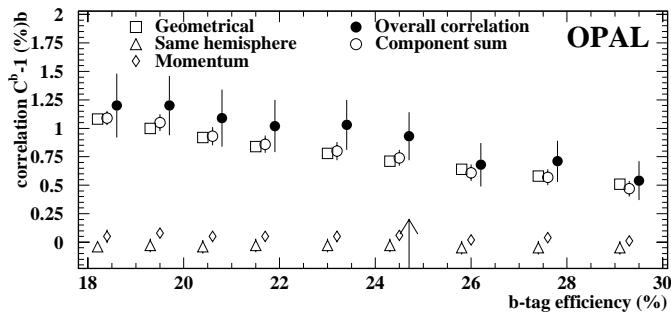**b hadron charged decay multiplicity:** The average charged decay multiplicity of the b hadrons was varied

Fig. 14. Comparison of the true overall tagging efficiency correlation and the various components for the combined vertex and lepton tag, as the b-tagging efficiency is varied by changing the vertex tag cut. The individual components are slightly displaced along the x-axis for clarity, and the analysis cut is shown by the arrow

by ± 0.35 using a weighting method. The size of the variation reflects the accuracy of the measurements by DELPHI and OPAL [40].

The resulting variations in the correlation coefficients are all rather small, and much smaller than the dominant uncertainties caused by momentum correlation effects.

8.8 Correlation completeness test

The sizes of the various components of the correlation in Monte Carlo, together with their associated statistical errors, are given in Table 8. The evolution of the various components as the b-tagging efficiency is varied is shown in Fig. 14. In the absence of interdependence between the correlation components, the values of $C^{\mathrm{b}} - 1$ from each component can be added to give the overall correlation. The sum of the components in Table 8 is compatible with the overall correlation evaluated from the ratio of the event tagging efficiency to the product of the hemisphere tagging efficiencies, for both vertex and combined tags. This strongly suggests that no large correlation contribution has been omitted from the systematic error evaluation, though the precision of this test is limited by the overall Monte Carlo statistics and by interdependence between the different components. In the previous analysis [4], an additional systematic error was included to cover such interdependence, since the overall correlation was determined by simply adding the components. No such error is included here, since the Monte Carlo is used to determine the value of the correlation directly, including any interdependence.

These correlation component sums have been made using the $C^{\mathrm{b}}_{p,\bar{p}}$ estimate from (4) for the momentum correlation. If the energy and momentum conservation $C^{\mathrm{b}}_{E,p}$ estimate from (6) is used instead, the component sums are $(0.63\pm0.05)\,\%$ and $(0.54\pm0.04)\,\%$ for the vertex and combined tags, still compatible with the overall Monte Carlo correlation. It should be emphasised that the central value used for the correlation does not depend on which method is used to evaluate the momentum correlation component.

Table 8. Components of the hemisphere efficiency correlation $C^{\mathrm{b}} - 1$ in $\mathrm{b\bar{b}}$ Monte Carlo events, together with their sum and the overall correlation in the Monte Carlo sample. Only statistical errors are included

Correlation $C^{\mathrm{b}} - 1$ (%)	Vertex	Combined
Same hemisphere events	0.02 ± 0.02	-0.03 ± 0.02
Momentum correlation	0.04 ± 0.05	0.06 ± 0.03
Geometrical correlation	0.88 ± 0.02	0.71 ± 0.02
Component sum	0.94 ± 0.06	0.74 ± 0.04
Overall correlation	0.83 ± 0.20	0.93 ± 0.17

9 Summary and conclusion

The fraction R_{b} of $\mathrm{Z}^0 \to \mathrm{b\bar{b}}$ events in hadronic Z^0 decays was measured using data collected by OPAL between 1992 and 1995 using tags based on displaced secondary vertices and identified leptons, giving the result

$$R_{\mathrm{b}} = 0.2178 \pm 0.0011 \pm 0.0013$$

where the first error is statistical and the second systematic. The systematic error does not include the effects of varying R_{c} from its Standard Model expectation. The result depends on R_{c} as follows:

$$\frac{\Delta R_{\mathrm{b}}}{R_{\mathrm{b}}} = -0.056 \frac{\Delta R_{\mathrm{c}}}{R_{\mathrm{c}}}$$

where ΔR_{c} is the deviation of R_{c} from the value 0.172 predicted by the Standard Model.

This result is in agreement with and supersedes our previous measurement [4]. It is also in agreement with other recent measurements at LEP [12,41] and SLC [42], and with the Standard Model prediction of 0.2155 ± 0.0003 [2].

References

1. See for example: P. Bamert et al., Phys. Rev. D **54**, 4275 (1996), and references therein
2. D. Bardin et al., CERN-TH 6443/92, May 1992. We use ZFITTER version 5.0 with default parameters, and the following inputs: $m_Z = 91.1867 \pm 0.0020$ GeV, $m_t = 175.6 \pm 5.5$ GeV, $\alpha(m_Z) = 1/128.909$, $\alpha_s(m_Z) = 0.120 \pm 0.003$ and $m_H = 115^{+116}_{-38}$ GeV
3. M.H. Seymour, Nucl. Phys. B **436**, 163 (1995)
4. OPAL collaboration, K. Ackerstaff et al., Z. Phys. C **74**, 1 (1997)
5. P.P. Allport et al., Nucl. Instrum. Methods **A346**, 476 (1994)
6. OPAL collaboration, K. Ahmet et al., Nucl. Instrum. Methods **A305**, 275 (1991); P.P. Allport et al., Nucl. Instrum. Methods **A324**, 34 (1993)
7. OPAL collaboration, R. Akers et al., Z. Phys. C **63**, 197 (1994)
8. T. Sjöstrand, Comp. Phys. Comm. **82**, 74 (1994)
9. OPAL collaboration, G. Alexander et al., Z. Phys. C **69**, 543 (1996)
10. C. Peterson, D. Schlatter, I. Schmitt and P. Zerwas, Phys. Rev. D **27**, 105 (1983)
11. J. Allison et al., Nucl. Instrum. Methods **A317**, 47 (1992)
12. ALEPH collaboration, R. Barate et al., Phys. Lett. B **401**, 150 (1997)
13. OPAL collaboration, P.D. Acton et al., Z. Phys. C **59**, 183 (1993); OPAL collaboration, R. Akers et al., Phys. Lett. B **338**, 497 (1994)
14. The neural networks were trained using JETNET 3: C. Peterson, T. Rögnvaldsson and L. Lönnblad, Comp. Phys. Comm. **81**, 185 (1994)
15. OPAL collaboration, R. Akers et al., Z. Phys. C **70**, 357 (1996)
16. OPAL collaboration, P.D. Acton et al., Z. Phys. C **58**, 523 (1993)
17. OPAL collaboration, K. Ackerstaff et al., CERN-EP/98-054, Eur. Phys. J. C **5**, 411 (1998)
18. ALEPH Collaboration, D. Buskulic et al., Z. Phys. C **62**, 179 (1994)
19. DELPHI collaboration, P. Abreu et al., Z. Phys. C **59**, 533 (1993), erratum in Z. Phys. C **65**, 709 (1995); OPAL collaboration, G. Alexander et al., Z. Phys. C **72**, 1 (1996)
20. ALEPH collaboration, D. Buskulic et al., Z. Phys. C **62**, 1 (1994); OPAL collaboration, R. Akers et al., Z. Phys. C **67**, 27 (1995)
21. The LEP collaborations, ALEPH, DELPHI, L3 and OPAL, Nucl. Instrum. Methods **A378**, 101 (1996). Updated averages are described in 'Presentation of LEP Electroweak Heavy Flavour Results for Summer 1998 Conferences', LEPHF 98-01 (see `http://www.cern.ch/LEPEWWG/heavy/`)
22. P. Collins and T. Spiller, J. Phys. **G11**, 1289 (1985)
23. V.G. Kartvelishvili, A.K. Likhoded and V.A. Petrov, Phys. Lett. B **78**, 615 (1978)
24. B. Anderson, G. Gustafson and B. Söderberg, Z. Phys. C **20**, 317 (1983)
25. ALEPH collaboration, D. Buskulic et al., Z. Phys. C **69**, 585 (1996)
26. Particle Data Group, C. Caso et al., Eur. Phys. J. C **3**, 1 (1998)
27. MARK III collaboration, D. Coffman et al., Phys. Lett. B **263**, 135 (1991)
28. Particle Data Group, R.M. Barnett et al., Phys. Rev. D **54**, 1 (1996)
29. ARGUS collaboration, H. Albrecht et al., Phys. Lett. B **278**, 202 (1992)
30. G. Altarelli et al., Nucl. Phys. B **208**, 365 (1982)
31. DELCO collaboration, W. Bacino et al., Phys. Rev. Lett. **43**, 1073 (1979)
32. MARK III collaboration, R.M. Baltrusaitis et al., Phys. Rev. Lett. **54**, 1976 (1985)
33. OPAL collaboration, R. Akers et al., Z. Phys. C **67**, 27 (1995); OPAL collaboration, R. Akers et al., Phys. Lett. B **353**, 595 (1995)
34. ALEPH collaboration, R. Barate et al., 'A measurement of the gluon splitting rate into $b\bar{b}$ pairs in hadronic Z decays', CERN-EP/98-103, Phys. Lett. B **434**, 437 (1998); DELPHI collaboration, P. Abreu et al., Phys. Lett. B **405**, 202 (1997)
35. OPAL collaboration, R. Akers et al., Z. Phys. C **67**, 389 (1995); OPAL collaboration, G. Alexander et al., Z. Phys. C **73**, 569 (1997); OPAL collaboration, G. Alexander et al., Z. Phys. C **73**, 587 (1997)
36. G. Marchesini et al., Comp. Phys. Comm. **67**, 465 (1992)
37. P. Nason and C. Oleari, Phys. Lett. B **407**, 57 (1997)
38. OPAL collaboration, M. Akrawy et al., Phys. Lett. B **253**, 511 (1990)
39. ALEPH Collaboration, D. Buskulic et al., Phys. Lett. B **357**, 699 (1995) ; DELPHI Collaboration, P. Abreu et al., Z. Phys. C **66**, 323 (1995); OPAL Collaboration, R. Akers et al., Z. Phys. C **60**, 199 (1993); OPAL Collaboration, G. Alexander et al., Phys. Lett. B **364**, 93 (1995)
40. DELPHI Collaboration, P. Abreu et al., Phys. Lett. B **347**, 447 (1995) ; OPAL Collaboration, R. Akers et al., Z. Phys. C **61**, 209 (1994)
41. ALEPH collaboration, R. Barate et al., Phys. Lett. B **401**, 163 (1997) ; DELPHI collaboration, P. Abreu et al., Z. Phys. C **70**, 531 (1996)
42. SLD collaboration, K. Abe et al., Phys. Rev. Lett. **80**, 660 (1998)